Satellite NO2 Trends and Hotspots over Offshore Oil and Gas Operations in the Gulf of Mexico

Niko Markovich Fedkin[1], Ryan Michael Stauffer[2], Anne M. Thompson[3], Debra E. Kollonige[4], HOLLI D WECHT[5], and Nellie Elguindi[6]

[1]Goddard Space Flight Center
[2]NASA Goddard Space Flight Center
[3]UMBC/JCET @ NASA-GODDARD
[4]NASA-gsfc
[5]bUREAU OF oCEAN eNERGY mGT
[6]Bureau of Ocean Energy Management

July 20, 2023

Abstract

The Outer Continental Shelf of the Gulf of Mexico (GOM) is populated with numerous oil and natural gas (ONG) platforms which produce NOx (NOx = NO + NO2), a major component of air pollution. The Bureau of Ocean Energy Management (BOEM) is mandated to ensure that the air quality of coastal states is not degraded by these emissions. As part of a NASA-BOEM collaboration, we conducted a satellite data-based analysis of nitrogen dioxide (NO2) patterns and trends in the GOM. Data from the OMI and TROPOMI sensors were used to obtain 18+ year records of tropospheric column (TrC) NO2 in three GOM regions: 1) Houston urban area, 2) near shore area off the Louisiana coast, and a 3) deepwater area off the Louisiana coast. The 2004-2022 time series show a decreasing trend for the urban (-0.027 DU/decade) and near shore (-0.0022 DU/decade) areas, and an increasing trend (0.0019 DU/decade) for the deepwater area. MERRA-2 wind and TROPOMI NO2 data were used to reveal several NO2 hotspots (up to 25% above background values) under calm wind conditions near individual platforms. The NO2 signals from these deepwater platforms and the high density of shallow water platforms closer to shore were confirmed by TrC NO2 anomalies of up to 10%, taking into account the monthly TrC NO2 climatology over the GOM. The results presented in this study establish a baseline for future estimates of emissions from the ONG hotspots and provide a methodology for analyzing NO2 measurements from the new geostationary TEMPO instrument.

Satellite NO_2 Trends and Hotspots over Offshore Oil and Gas Operations in the Gulf of Mexico

Niko M. Fedkin[1,3], Ryan M. Stauffer[1], Anne M. Thompson[1,2], Debra E. Kollonige[1,3] , Holli D. Wecht[4], Nellie Elguindi[4]

[1]Earth Sciences Division, NASA/Goddard Space Flight Center, Greenbelt, MD, USA
[2] GESTAR and Joint Center for Earth Systems Technology, University of Maryland, Baltimore County, Baltimore, MD, USA
[3] SSAI., Lanham, MD, USA
[4]Bureau of Ocean Energy Management, Office of Environmental Programs, Sterling, VA, USA

Corresponding author: Niko Fedkin (niko.m.fedkin@nasa.gov)

Key Points:

- Satellite NO_2 records and trends of urban, coastal and deep water areas from 2005 to 2022, are presented
- Classifying NO_2 over the Gulf of Mexico (GOM) under various wind conditions highlights typical patterns in average NO_2 values
- GOM NO_2 hotspots from deepwater platforms were identified by TROPOMI under calm wind conditions, the largest of which is over Mars/Olympus

Abstract

The Outer Continental Shelf of the Gulf of Mexico (GOM) is populated with numerous oil and natural gas (ONG) platforms which produce NO_x ($NO_x = NO + NO_2$), a major component of air pollution. The Bureau of Ocean Energy Management (BOEM) is mandated to ensure that the air quality of coastal states is not degraded by these emissions. As part of a NASA-BOEM collaboration, we conducted a satellite data-based analysis of nitrogen dioxide (NO_2) patterns and trends in the GOM. Data from the OMI and TROPOMI sensors were used to obtain 18+ year records of tropospheric column (TrC) NO_2 in three GOM regions: 1) Houston urban area, 2) near shore area off the Louisiana coast, and a 3) deepwater area off the Louisiana coast. The 2004-2022 time series show a decreasing trend for the urban (-0.027 DU/decade) and near shore (-0.0022 DU/decade) areas, and an increasing trend (0.0019 DU/decade) for the deepwater area. MERRA-2 wind and TROPOMI NO_2 data were used to reveal several NO_2 hotspots (up to 25% above background values) under calm wind conditions near individual platforms. The NO_2 signals from these deepwater platforms and the high density of shallow water platforms closer to shore were confirmed by TrC NO_2 anomalies of up to 10%, taking into account the monthly TrC NO_2 climatology over the GOM. The results presented in this study establish a baseline for future estimates of emissions from the ONG hotspots and provide a methodology for analyzing NO_2 measurements from the new geostationary TEMPO instrument.

Plain Language Summary

Oil and natural gas operations emit nitrogen oxides (NO_x), which are major air pollutants and precursors to ground-level ozone. The Bureau of Ocean Energy Management (BOEM) agency is responsible for managing planned oil and natural gas (ONG) activity on the outer continental

shelf, and is mandated to ensure related emissions do not degrade air quality of coastal states. In collaboration with BOEM, we used satellite data from the OMI and TROPOMI sensors to construct an 18+ year record of tropospheric nitrogen dioxide (NO_2), a proxy for NO_x, in the Gulf Coast region. These time series focused on three areas: 1) Houston urban, 2) off the Louisiana coast, and 3) deepwater Gulf off Louisiana. These regions experienced changes in tropospheric column NO_2 of -13.7%, -5.8% and +5.4% per decade, respectively. We also identified NO_2 hotspots from ONG platforms using TROPOMI NO_2 averages under calm wind conditions. The ONG deepwater platforms enhance NO_2 background amounts by 7-13% on average, and up to 25% for the Mars and Olympus platforms combined. The results presented here will facilitate our work on emissions estimates from these sources and on applications to the recently launched TEMPO instrument.

1. Introduction

Nitrogen dioxide (NO_2), a component of NO_x ($NO_x = NO + NO_2$) and classified as a criterion pollutant by the Environmental Protection Agency (EPA), is produced from fuel combustion. Anthropogenic sources of NO_2 include fires, vehicular emissions, power plants and other industrial activities such as oil and natural gas (ONG) production. In large quantities, NO_2 causes respiratory problems from prolonged exposure. Furthermore, NO_2 is a major precursor to tropospheric ozone (O_3), another criteria pollutant responsible for damaging effects on lungs and premature mortality (Bell et al., 2006). Amounts of NO_2 are measured with in-situ analyzers, typically reporting in mixing ratio, or through remote sensing instruments that report column amounts. Ground-based remote sensors for total column NO_2 (TC NO_2, Piters et al., 2012) include the Pandora spectrometer (Herman et al., 2009). Airborne remote sensors, e.g., the Geo-CAPE Airborne Simulator (GCAS) (Nowlan et al., 2018; Judd et al., 2019) and the Geostationary Trace gas and Aerosol Sensor Optimization (GEO-TASO) (Nowlan et al., 2016) measure the NO_2 column amount below the aircraft. From space, TC NO_2 is measured with satellite ultraviolet-visible (UV-Vis) sensors. A long TC NO_2 record exists thanks to a series of satellite sensors: the Global Ozone Monitoring Experiment (GOME, Burrows et al., 1999; Richter et al., 2002) and GOME-2 (Richter et al., 2011; Munro et al., 2016) instruments, the Ozone Monitoring Instrument (OMI) (Levelt et al., 2006; Levelt et al., 2018), and the Tropospheric Monitoring Instrument (TROPOMI) instrument launched in 2017 (Van Geffen et al., 2012). TROPOMI also supplies a tropospheric column (TrC) NO_2 product, which has been used for a range of air quality applications.

Satellite instruments are very useful for providing column NO_2 data over areas without surface monitoring, especially over water. Over the past decade a number of studies have compared satellite TC NO_2 with both in-situ and remotely sensed NO_2 in coastal areas. Land-sea interactions, e.g., sea-breeze and other dynamical factors, show how challenging satellite NO_2 validation can be over both sides of the land-water interface. The Korea-United States Ocean Color experiment (KORUS-OC) (Tzortziou et al., 2018; Thompson et al., 2019), around the Korean Peninsula in 2016, found that complex interactions of advected pollution and meteorology determined whether satellite TC NO_2 column amounts correlated with shipboard Pandora TC NO_2 and in-situ NO_2 measurements. Similarly, the Ozone Water-Land Environmental Transition Study (OWLETS) projects over the southern Chesapeake Bay region in 2017 (Sullivan et al., 2018; Dacic et al., 2020) and near Baltimore in 2018 (Sullivan et al., 2020; Kotsakis et al., 2022) discovered that the accuracy of satellite TC NO_2 data depended on resolution (pixel size), cloud-cover, pollution amount and whether the satellite was measuring

over land or water. Other campaigns with TC NO_2 measurements in coastal areas include DISCOVER-AQ in Baltimore (2011) (Ttzortiou et al., 2013; Reed et al., 2015) and Houston (2013) (Judd et al., 2019; Choi et al., 2020), and the Deposition of Atmospheric Nitrogen to Coastal Ecosystems (DANCE) campaign in (Martins et al., 2016; Kollonige et al., 2019).

In the Gulf of Mexico (GOM), a notable source of NO_x is from ONG exploration and production sites. The above-mentioned campaigns, while investigating air quality in coastal regions, did not focus on areas of concentrated offshore ONG activity or validation of satellite NO_2 near ONG sources. We addressed these issues in a 3-year study that NASA undertook in collaboration with the Bureau of Ocean Energy Management (BOEM, Department of Interior). BOEM is the agency responsible for managing ONG exploration, development, and production plans in the U.S. Outer Continental Shelf (OCS). The agency specifically has air quality jurisdiction for OCS emissions from ONG exploration and development to the west of 87.5°. It is also mandated to ensure that criteria pollutant emissions from these activities are in compliance with the national ambient air standards to the extent that the activities do not significantly affect the air quality of any state. BOEM tracks industry-reported NO_x emissions from ONG operations in monthly inventories (Wilson et al., 2018). However, due to lack of air quality monitoring on the OCS, the reported emissions remain unvalidated. NASA and BOEM carried out a feasibility study from 2017 to 2020 to determine whether satellite data could be used to monitor NO_2 over the GOM and discriminate regional sources and/or resolve pollution from individual platforms. Preliminary results were summarized in two documents by Duncan (2020) and Thompson (2020). These were followed by detailed reports on a 2019 field campaign (Satellite Coastal and Oceanic Atmospheric Pollution Experiment), SCOAPE-I (Thompson, 2020; Thompson et al., 2023), along the Louisiana coast.

The SCOAPE-I cruise took place 10-18 May 2019 aboard the *Research Vessel Point Sur*. One of the goals of this campaign was to measure in-situ NO_2 levels along the Louisiana coast with a cruise track designed to sample smaller near-shore ONG operations, over open water, and near large deepwater ONG platforms farther away from the coast. The deepwater platforms primarily produce oil and flare excess gas; thus, they usually have larger individual platform NO_x emissions. For NO_2, the *Point Sur* was equipped with a NO_2 in-situ analyzer and a Pandora spectrometer for measuring TC NO_2 amounts. Pandora measurements were taken during daytime in cloud-free conditions. Measurements of NO_2 were also collected with Pandora, satellites, and an NO_2 analyzer at the Louisiana Universities Marine Consortium (LUMCON; Cocodrie, LA; 29.26°, 90.66°) SCOAPE-I port during the cruise and the three weeks prior.

During the SCOAPE I cruise, satellite (OMI, TROPOMI) and the shipboard Pandora total column (TC) NO_2 levels were elevated in the vicinity of ONG platforms as confirmed by numerous coincident NO_2 spikes from the shipboard analyzer. However, neither the satellite nor Pandora TC NO_2 responses to emissions were as large as surface NO_2 increases. Comparisons between NO_2 column amounts from satellite and surface Pandoras showed good agreement during SCOAPE I - within 13% over water and 5% over land in clear sky conditions - and NO_2 signals from selected ONG platforms could sometimes be isolated (Thompson et al., 2023). However, consistent quantification of NO_2 sources was not possible due to cloud cover, satellite sampling frequency (one overpass daily) and relatively coarse spatial resolution compared to platform size, factors all amplified by the short duration of the cruise. Two air quality regimes, differentiated by prevailing wind direction, were characterized by surface and satellite measurements during SCOAPE I: clean marine air over deepwater (onshore wind from remote marine locations) and polluted continental air near shore (wind from land). In between, elevated NO_2 near-shore can result from nearby pollution, from deepwater regions <u>*or*</u> from the continent.

There is now nearly five years of TROPOMI and 18+ years of OMI observations, both TC NO_2 and TrC NO_2. This prompts us to conduct a more comprehensive study of satellite NO_2 over the GOM, examining regional and temporal variability. We use OMI and TROPOMI TrC NO_2 data to: 1) analyze the long-term NO_2 record over three prototype regions within the GOM and 2) identify NO_2 hotspots near ONG operations using wind-classified TROPOMI data. The longer time-series are used to determine trends in NO_2. Anomalous calm-wind TROPOMI data pinpoint major and lesser-emitting platforms. The results, summarized in Section 3.1 and 3.2, provide a baseline for the longer-term goal of monitoring GOM ONG NO_x emissions. Identifying the hotspots is crucial for BOEM's mission and demonstrates the ability to monitor ONG pollution with remote sensing instruments in anticipation of the geostationary Tropospheric Emissions: Monitoring of Pollution (TEMPO) data. The results for this second objective are found in Section 3.3.

2. Methodology

2.1 Description of study domain

The focus area is the Outer Continental Shelf (OCS) of the Gulf of Mexico (GOM), an area populated with numerous oil and natural gas platform operations (Figure 1). There are two main types of platforms: shallow water and deepwater platforms. Deepwater platforms are further from the coast, more isolated, and produce NO_x emissions due to gas flaring. Shallow water platforms generally produce less NO_x than deepwater platforms but are greater in density near the shore. The majority of the platforms in the GOM produce less than 1000 metric tons of NO_2 per year with exception of the deepwater platforms away from shore, according to the 2017 BOEM inventory (Figure 1; Wilson et al., 2018). The domain of this study is between 25°N and 30° N latitude and 95° W and 87.5° W longitude. This includes most of the OCS of the GOM over which BOEM has jurisdiction (200 nautical miles beyond state jurisdictions). We also consider the Houston, TX, urban area as a reference in comparison to the areas over water. In particular, Houston was chosen because it is the highest NO_x emitting region along the Gulf coast and has been the location of multiple air quality campaigns such as DISCOVER-AQ (Judd et al., 2019; Nowlan et al., 2018; Choi et al., 2020) and TRACER-AQ in 2021 (Jensen et al., 2022; Judd et al., 2021).

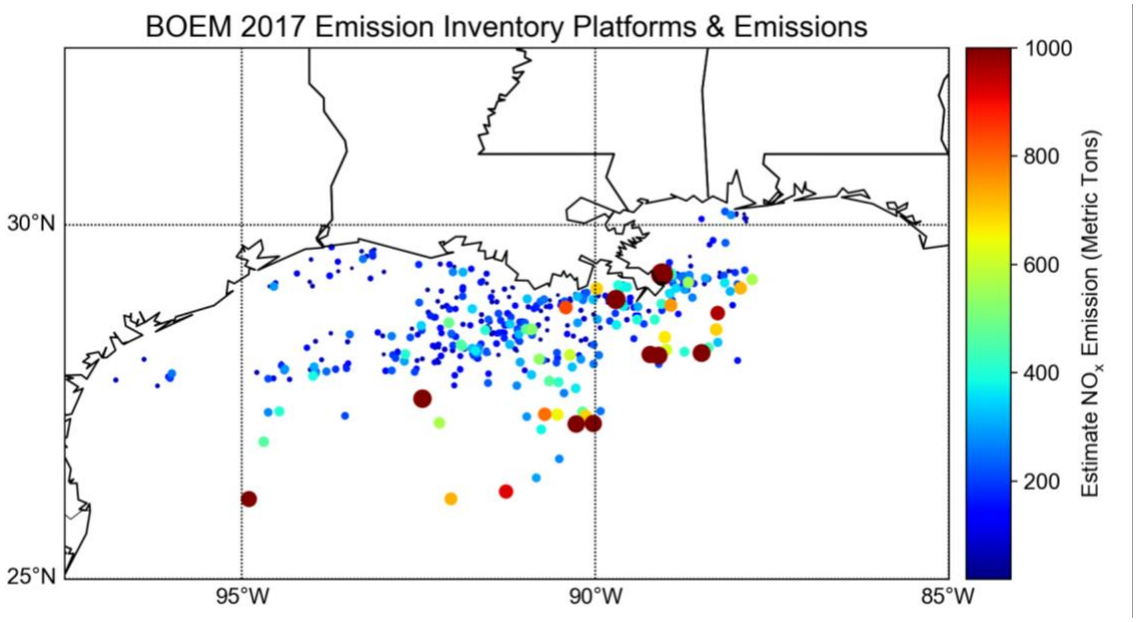

Figure 1: Locations of the Gulf of Mexico ONG platforms in the BOEM 2017 emission inventory. Larger dots and corresponding colors indicate the platforms with the highest annual NO_x emissions.

The study domain was further divided into smaller regions to compare areas that are expected to have contrasting NO_x emissions and observed NO_2 amounts. A deepwater area, a near shore area and an urban area were defined and shown as a green, red and orange box in Figure 2, respectively. The near shore area covers parts of both BOEM (federal) and Louisiana state jurisdictions, and includes numerous shallow water platforms within about 100 km from the Louisiana coast. The latitude bound of the near shore area is 28.3° N and 29.3° N in this analysis. The defined deepwater area is between 27° and 28.3° N and includes several deepwater operations with NO_x emissions greater than 500 metric tons. In this study, the deepwater area can also be treated as being close to background NO_2 levels, since marine air is clean and the deepwater platforms are relatively isolated.

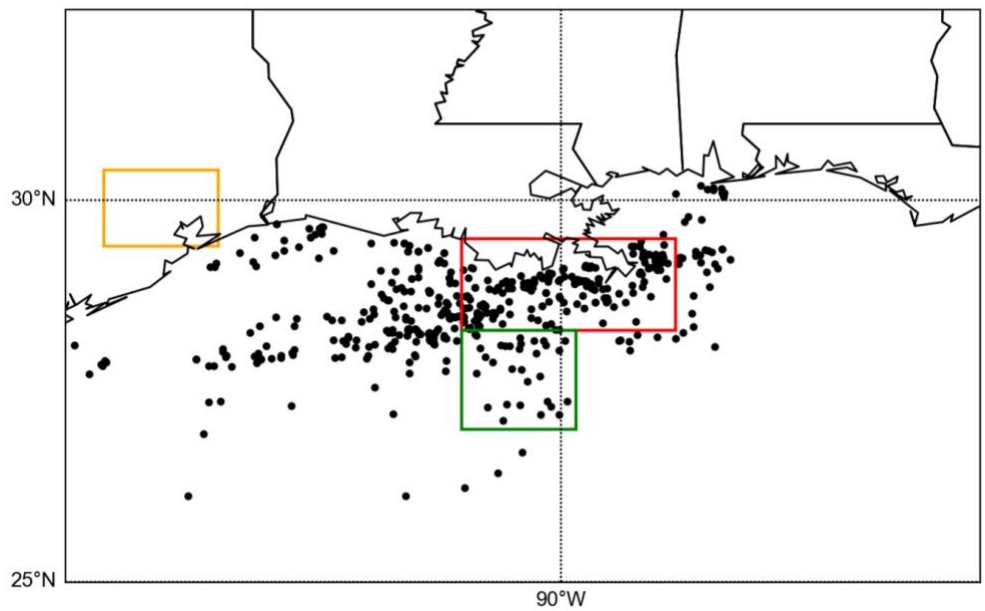

Figure 2: Map of the three areas of focus for which OMI and TROPOMI time series are calculated: Shallow water off the east Louisiana coast (red box), GOM deepwater (green box) and Houston, TX, metropolitan area (orange box). Each black dot represents a platform or facility in the BOEM OCS 2017 emissions inventory.

2.2 Datasets

For this work, we used satellite datasets from the Ozone Monitoring Instrument (OMI) (Levelt et al., 2006; Levelt et al., 2018) and TROPOMI (Veefkind et al., 2012). Located onboard NASA's polar orbiting Aura satellite, OMI was launched in 2004 and its data record began in October of that year. OMI collects observations over a particular location about once a day at a spatial resolution of 13 x 24 km^2 at nadir and 24x160 km^2 at the edge of the swath. The satellite is sun synchronous and makes an overpass at around 1300-1400 local time. In this study we use the high-resolution OMI Tropospheric NO_2 Version 4 dataset (Lamsal et al., 2021; https://avdc.gsfc.nasa.gov/pub/data/satellite/Aura/OMI/V03/L3/OMNO2d_HR), which contains several improvements to air mass factors (AMFs) compared to Version 3. In particular, this version incorporates improved cloud algorithms, a geometric Lambertian Equivalent Reflectance (GLER) product and improved terrain pressure calculations into the NO_2 retrieval. This Level 3 (L3) gridded research product has a resolution of 0.1° × 0.1° – an increase from the 0.25° × 0.25° of the original Level 3 dataset. At times the spatial coverage of OMI is impacted by the row anomaly (Torres et al., 2018), a physical instrument issue which obstructs some of the instrument's field of view and therefore affects radiance measurements.

The TROPOMI instrument was launched by the European Space Agency on the European Union's Copernicus Sentinel 5 Precursor (S5P) satellite in October 2017, with the data record beginning May 2018. The overpass of TROPOMI occurs in early afternoon, within about 0.5 hr. of OMI. The resolution of the instrument is currently 3.5 × 5.6 km^2 at nadir (3.5 × 7 km^2 prior to August 2019). Like other polar orbiting instruments, TROPOMI provides daily global coverage, although only about once per day at any given location. TROPOMI's NO_2 algorithms use a differential optical absorption spectroscopy (DOAS) technique on radiances in the 405–465 nm spectral window. The spectral radiances are converted into slant column

densities (SCD) of NO_2 between the instrument and the Earth's surface (van Geffen et al., 2020). AMFs are then used to convert the slant column into a vertical column density (VCD). For obtaining the tropospheric NO_2 column, the stratospheric portion is subtracted from the total SCD using global model estimates (Boersma et al., 2004; Boersma et al., 2007). The algorithms have been updated throughout the course of TROPOMI's operation, resulting in multiple versions of the data. The research dataset S5P-PAL (https://data-portal.s5p-pal.com/products/no2) was developed to apply the new algorithm (v2.3) to the older radiances, essentially homogenizing the data with respect to retrieval differences.

Lastly, we use the Modern Era Retrospective Analysis for Research and Applications Version 2 (MERRA-2, Gelaro et al., 2017) for wind analysis incorporated into calculating the satellite NO_2 time series. MERRA-2 is derived from the GEOS-5 data assimilation system and contains meteorological variables on a 0.5°× 0.625° grid for 42 standard pressure levels. The variables used in the analysis are the U and V components of the wind which are used to derive vector wind speed and direction.

2.3 Satellite NO_2 Time Series

The time series in this work consist of monthly averages of TrC NO_2. For OMI, a monthly version of the L3 high-resolution dataset is already available as a research product. The TROPOMI data were compiled by finding all overpasses over our study region in that month, re-gridding each daily file to a 0.01° × 0.01° grid and calculating the average for each grid point. The recommended quality assurance (QA) value of 0.75 was used as a threshold for filtering bad quality pixels. Next, the grid cells in each area previously described (deepwater, near shore and urban) were averaged for each month to obtain the time series for that particular region. From the resulting time series of monthly averages we also calculated the 12 month moving averages to account for the seasonality in the NO_2 time series. A trend line was fitted to the moving average to obtain an overall linear trend over the full record. The trends are presented in Section 3 along with the 95% confidence intervals.

Since meteorological regimes drove much of the variability in TC NO_2 in coastal areas during SCOAPE-I (Thompson et al., 2023), we also analyzed how the time series differ according to different wind speed and directions (source regions). For this objective, daily MERRA-2 wind data from 2005-2022 were used to restrict the NO_2 averaging to days based on three cases: 1) Wind from the north (land) at greater than 10 ms^{-1} 2) wind from the south (GOM) at greater than 10 ms^{-1} and 3) calm winds of less than 5 ms^{-1}. The 10 ms^{-1} threshold was chosen to ensure that sufficient transport was occurring that day within the lower levels of the atmosphere. For the north and south wind conditions, we defined the degree bounds as 120° to 240° and 300° to 60°, respectively. Note that here we use meteorological wind directions where due north is 360°. For the calm wind case, all wind directions are considered. It is important to note that 140-160 days out of the year are ignored, such as those with wind speeds between 5 and 10 ms^{-1}. For the Houston, TX box, the wind direction bounds were rotated by 45° counterclockwise in order to account for orientation of land and sea with respect to the city. The overall objective of this analysis was to determine how much the NO_2 column amount averages differ based on land vs. marine source regions, as well as cases with calm conditions and less regional transport. The MERRA-2 winds were evaluated for all MERRA-2 grid points within each box in Figure 2. A specific day was categorized if the wind direction was within the degree bounds and wind speed condition was met at all points. The 950 hPa pressure level was used because we are generally interested in the wind in the boundary layer but not specifically at the surface in the case that there is transport occurring aloft. The model surface winds also tend to

carry more uncertainty than at levels aloft. To best coincide with the overpass of OMI and TROPOMI, we only used the wind information at 18 UTC (12-1 pm local time).

Once the sets of days corresponding to each wind criterion were compiled, 3-month averages were computed from those days for each NO_2 time series. Three-month periods were used to account for sample size issues; some months have too few days of a wind criterion being met. For example, calm winds are more common in the summer than winter according to the climatology compiled from the MERRA-2 data (Figure 3). Aside from using the selected days for each case, the procedure for averaging the TROPOMI Level 2 (L2) and OMI L3 gridded data files was the same. This analysis yielded three time series for each area, corresponding to the three wind criteria. These results and their implications are discussed in Section 3.

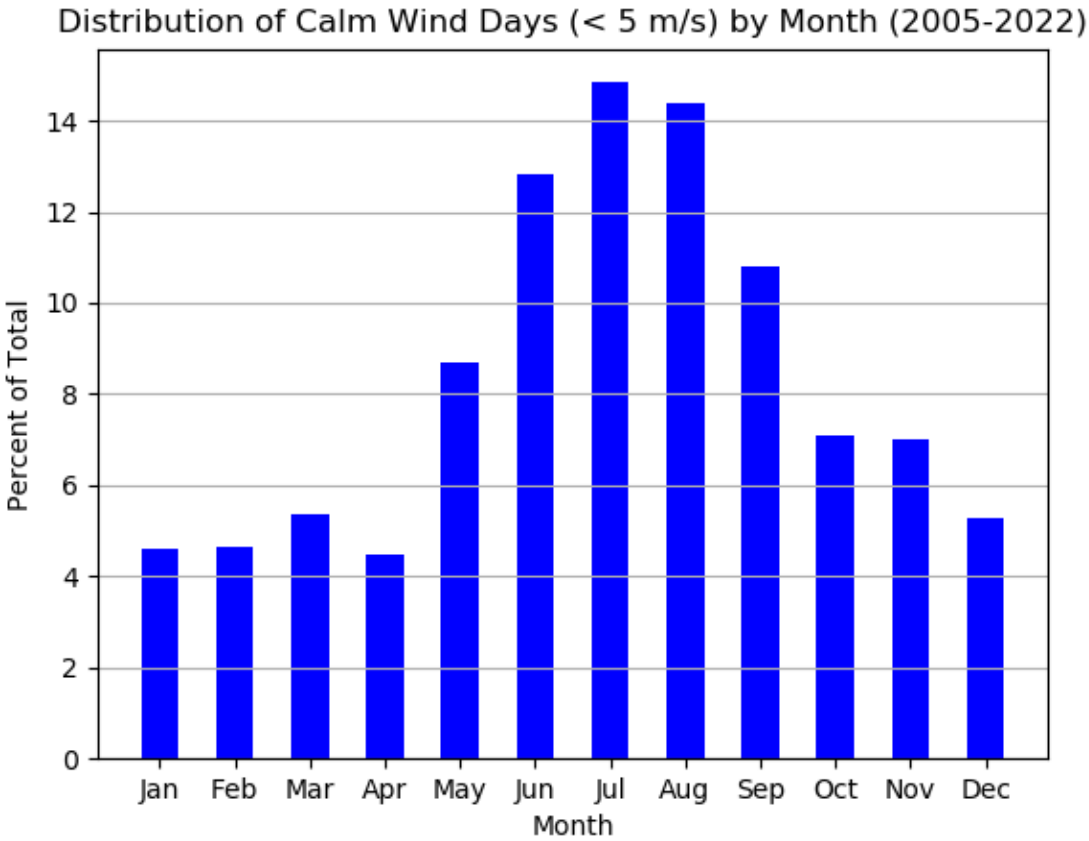

Figure 3: Distribution of number of days for each month for which the MERRA-2 950 hPa wind evaluated in the near shore area was less than 5 ms^{-1} (calm wind case). It is expressed as a percentage of the total number of days over the 18 years of the OMI record (2005 through 2022).

2.4 TROPOMI NO_2 Averages and Anomalies

The wind-based averaging was extended to TROPOMI data, with the goal of identifying NO_2 hotspots. This was done on an annual basis by calculating an average of all days in each year that fit the calm wind case (winds < 5 ms^{-1}). The maps with average TrC NO_2 are shown and described in Section 3.3. The same quality assurance threshold (0.75) and re-gridding technique was used as for the complete TROPOMI time series. To account for seasonality and differences in NO_2 between months, we also calculated TROPOMI NO_2 anomalies for 2018-2022. The first step was computing a climatology for every month by averaging all days during

the TROPOMI record for each individual month. Next, we separated the calm wind days by month and for each calculated the percent TrC NO_2 difference between the individual day and the climatology for the same month. Over the roughly 4.5 years of TROPOMI's data record, there were 450 individual calm wind day NO_2 anomalies calculated. An average was taken of this set of anomalies to obtain a single gridded anomaly (see Section 3.3) that describes the enhancement or reduction of NO_2 over each grid cell that also accounts for seasonal changes in NO_2 amounts.

3. Results

3.1 Satellite NO_2 Time Series

Figure 4 shows the 2004-2022 OMI time series for the three boxes defined in Figure 2. The red dashed trend lines were calculated from the 12-month moving averages to remove NO_2 seasonality. In the Houston, TX area (Figure 3a), the time series exhibits large seasonal fluctuations, in most cases over a factor of two from the winter to summer months. This is typically due to the differences in NO_2 lifetime in winter and summer months. The lifetime varies from 2 to 5hr during the daytime in summer (Beirle et al., 2011) and 12–24 hr during winter (Shah et al., 2020). The amplitudes of the peaks are noticeably higher in the first four years (2005-2009) of the time series compared to the most recent decade. There is an overall negative trend of -0.027± 0.0055 DU per decade with 13.7% decrease per decade, much of it due to the reduction of NO_2 in the first 5 years of the time series. Similar trends are also observed in urban areas throughout the U.S (Lamsal et al., 2015; Krotkov et al., 2016, Goldberg et al., 2021). After 2010, the NO_2 remains relatively constant. Over the entire time series the average value is 0.153 DU and this average value is closer to the minima of the NO_2 annual cycles due to the troughs of the annual cycle lasting several months, as opposed to 1-3 month peaks in winter.

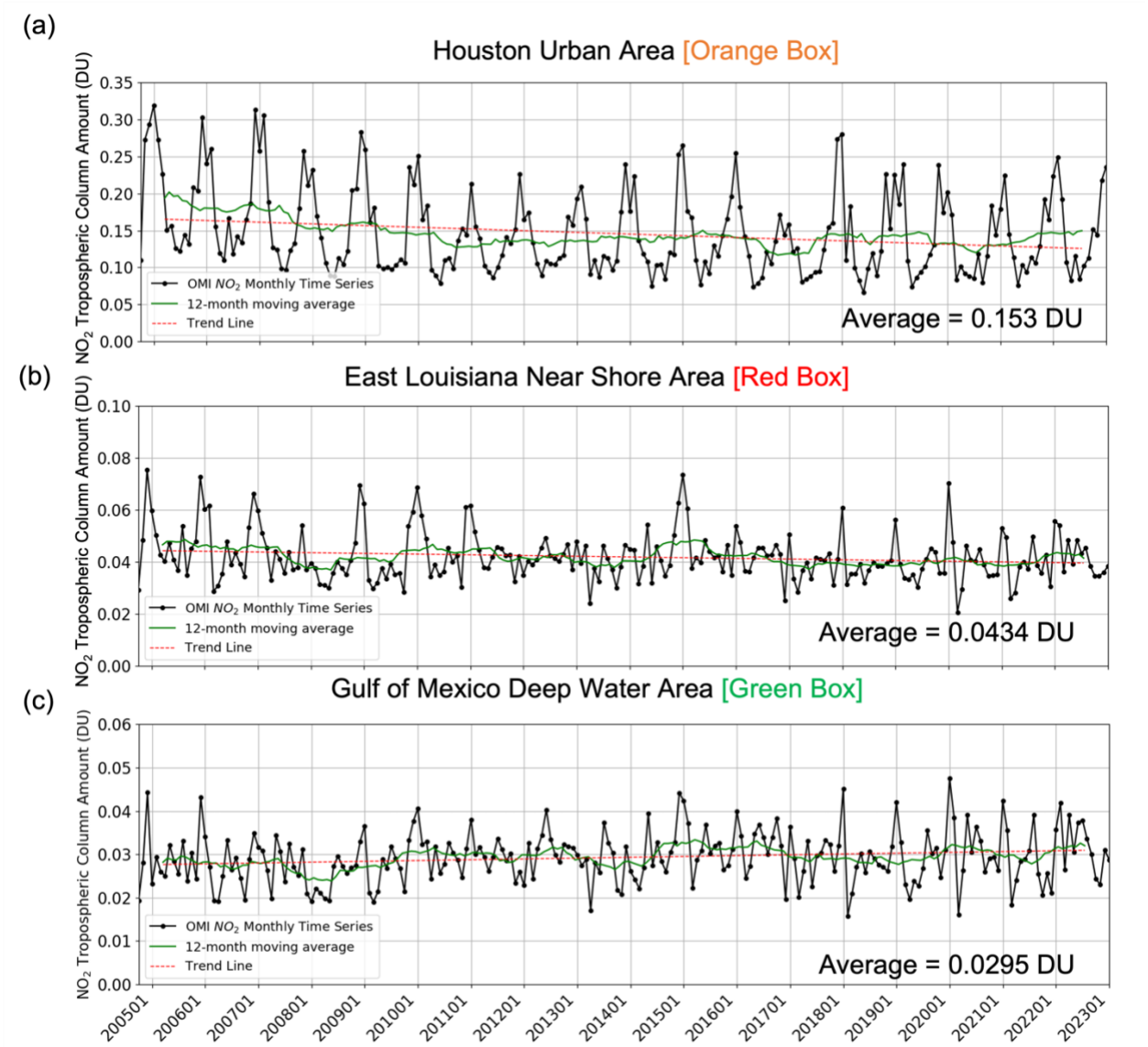

Figure 4: Time series of OMI TrC NO_2 monthly averages for the boxes shown in Figure 2, between late 2004 and 2022: (a) Houston, TX urban area (orange on Figure 2), (b) Near-shore (red on Figure 2), (c) GOM deepwater area in the GOM (green on Figure 2). The 12-month moving average (green line) and the linear trend line (dashed red) over the time series are also plotted.

Unlike the urban area, in the near shore area (Figure 4b) there is a less-defined NO_2 seasonality at the coast and over water. Although peaks and troughs in column NO_2 exist in 2005-2010, thereafter the time series becomes highly variable from month to month. The trend in this region was -0.0022± 0.0008 DU per decade (5.8% decrease per decade), and while still negative, is a lower magnitude than that of Houston by a factor of 10. The negative trend indicates the influence of relatively polluted land areas to the north, such as New Orleans; however, with fewer significant local sources, the potential for trends resulting from NO_2 emissions reductions is lower over-water. The average value for the near shore region is 0.0434 DU, about 28% of the urban Houston area value. It is important to note that while OMI can be

useful for remote sensing over water (e.g., Thompson et al., 2023), the data tend to be noisy on a day to day basis.

The deepwater area is characterized by a noisy time series with no discernable seasonal pattern (Figure 4c). Since all pixels in the box are used to calculate the average column amount value for each month, the influences of deepwater ONG operations in this area, which are relatively small compared to the pixel size, are likely washed out. In Section 3.3 we also show time series for NO_2 hotspots over individual ONG platforms without including the rest of the deepwater area. The overall average value in the deepwater area was 0.0295 DU, around 67% that of the near shore area and 19% of Houston. There is a slight increase of 5.4% per decade in this area with a positive trend (0.00189± 0.00054 DU per decade). The positive trend may result solely from noise due to the low NO_2 column amounts. However, we also note that there was an increase in deepwater ONG operations in the last decade which could have contributed to this trend (Section 3.3). Only the Houston trend is statistically significant given that the 95% confidence interval indicates an error uncertainty of 5.5%. For the near shore and deepwater areas, the uncertainty is around 30% for each. Given the higher uncertainty and smaller trend values, we cannot make a conclusive determination on whether the ONG activity drives these trends.

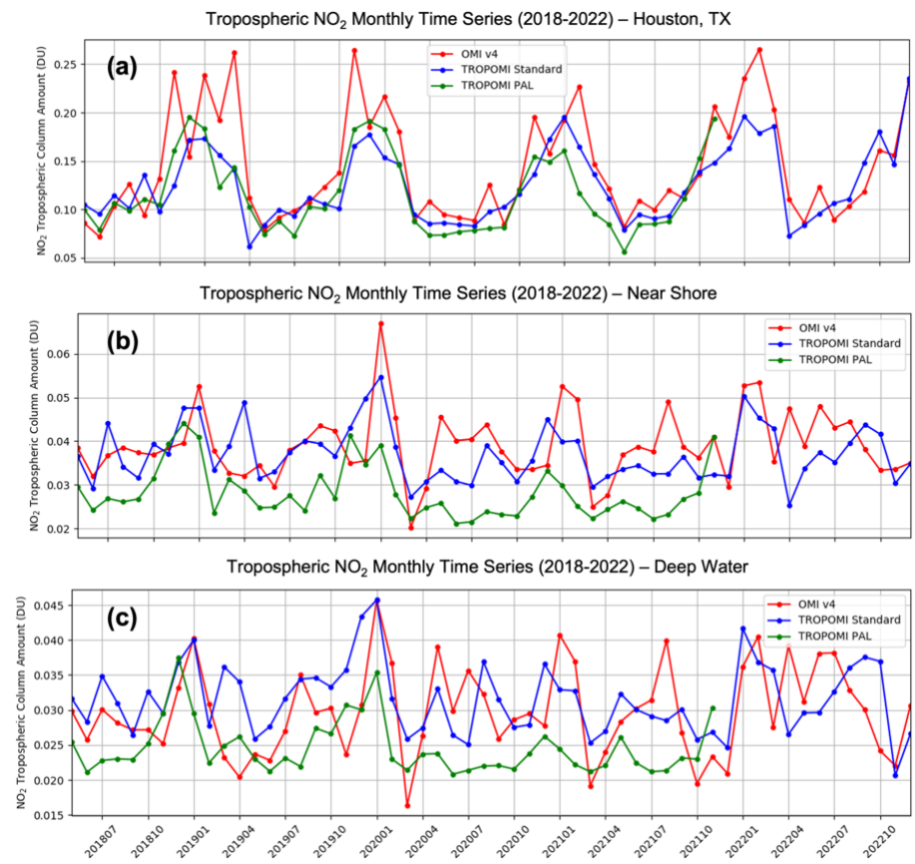

Figure 5: Comparisons of the 2018-2022 TrC NO_2 time series from OMI v4, the standard TROPOMI product and the reprocessed TROPOMI PAL product for a) Houston, TX urban area, (b) Near-shore, (c) GOM deepwater area in the GOM. Note that the TROPOMI PAL dataset is currently only available through 2021.

We calculated the NO_2 time series from all three satellite datasets over our three regions to provide context for the values described above. The time series of OMI, standard TROPOMI, and the TROPOMI PAL datasets (Figure 5) from 2018-2022 show how the observations differ. OMI averages 7.5% and 4.5% higher than TROPOMI in the near shore (Figure 5b) and deepwater areas (Figure 5c), respectively. This makes sense given that in the urban area OMI is clearly higher than TROPOMI observations on average (Figure 5a). These time series also show that the standard TROPOMI product is consistently higher than the PAL by around 21.5% in the deepwater box and 15.7% in the near shore box. The difference between the PAL and standard TROPOMI dataset was not found to be large over a polluted area like Houston, with the standard product being on average within 10% of the PAL between mid-2018 and late 2021.

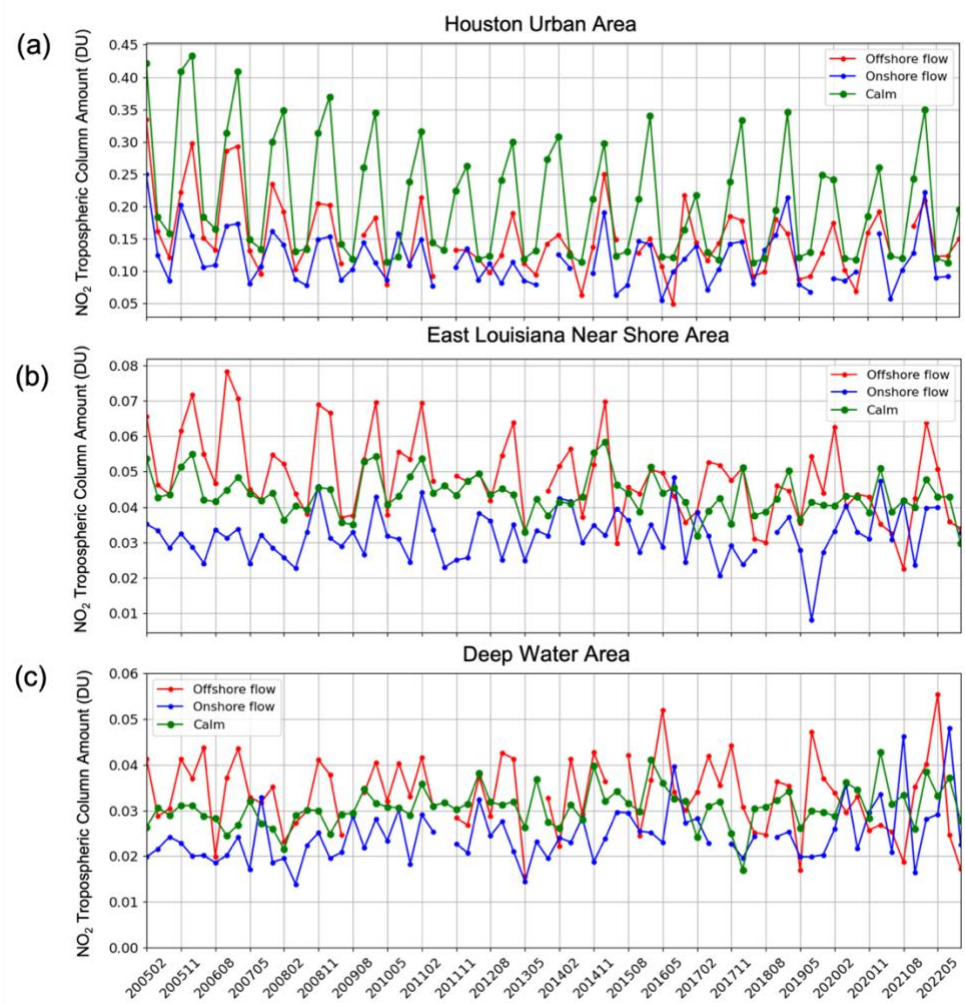

Figure 6: Time series of OMI TrC NO_2 seasonal averages based on wind condition, for: (a) Houston, TX urban area, (b) Near-shore, and (c) GOM deepwater area. The three conditions for (b) and (c) are: MERRA-2 950 hPa winds > 10 ms^{-1} from the south quadrant (blue line), winds > 10 ms^{-1} from the north quadrant (red line) and winds less than 5 ms^{-1} from any direction (green line). For (a), the directions were adjusted to southwest (blue) and northwest (red) quadrants respectively.

3.2 Wind-based Time Series

The time series, with the influence of different wind conditions described in Section 2, are displayed in Figure 6. Missing points are the 3-month time periods when there were not enough days to meet the wind conditions (at least 10). For the Houston area (Figure 6a), calm winds clearly result in the highest average NO_2 column amount (0.207 DU) because there is little transport of emissions away from the city. This is about a 35% increase above the average of the entire Houston time series (Figure 4a). Offshore flow (wind from other land areas toward the GOM) produces an average monthly column amount of 0.151 DU, while onshore flow results in an average value of 0.118 DU. This indicates that for the most part offshore sources do not impact onshore areas given their small magnitude of NO_x emission. As expected, in the near shore and deepwater areas (Figure 6b and 6c), the calm wind time series fall in between the offshore and onshore wind time series. The trends of the calm wind case in near shore and deepwater areas are -0.0027 DU per decade and 0.0021 DU per decade respectively. Although these NO_2 amounts and trends are relatively small, this equates to a total increase of 13.5% for the deepwater area, and 8.5% decrease for the near shore area over the OMI record. The NO_2 trends corresponding to calm wind conditions can also better describe trends over ONG operations since we eliminate days with significant transport of clean or polluted air masses. Average TrC NO_2 amount for the onshore flow case in the deepwater was 0.024 DU which can be considered very close to a typical background value over clean marine areas. For the calm wind case the average value was 0.032 DU, only slightly lower than the offshore case (0.0335 DU). The small difference between the two can be partially explained by the significant dip in 2020 for the offshore flow case, most likely due to the COVID-19 lockdowns. Table 1 summas the average column amounts for the original time series and wind-based time series. For the near shore and deepwater areas, the calm wind time series averages were close to the overall average.

Table 1: Average OMI Column TrC NO_2 for the wind-based time series and the original time series.

Time Series NO_2 Tropospheric Column Amount Averages (DU)

Wind condition	Urban	Near shore	Deepwater
Offshore flow	0.151	0.0495	0.0335
Onshore flow	0.118	0.0307	0.0231
Calm	0.209	0.0440	0.0307
None (all days)	0.153	0.0434	0.0295

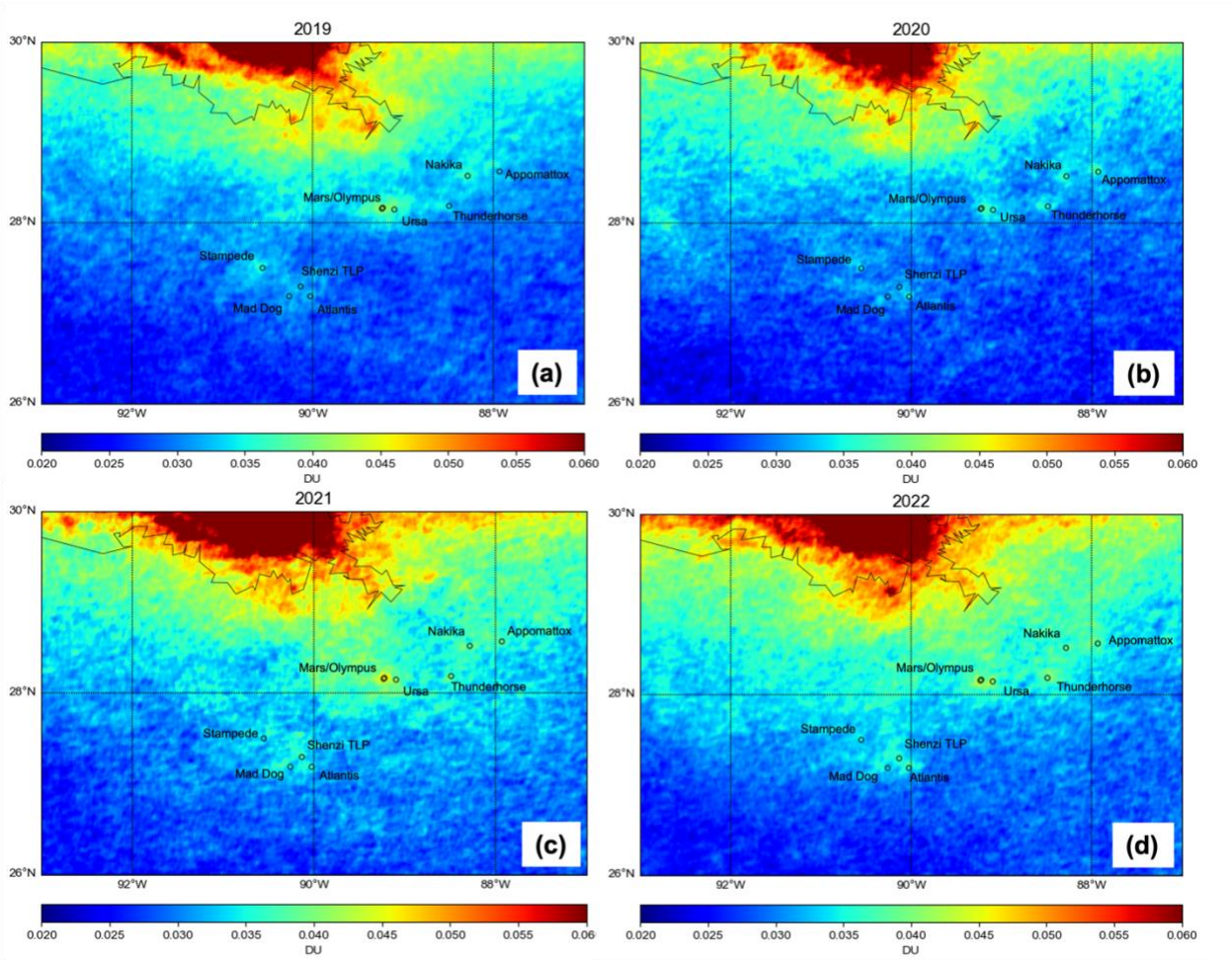

Figure 7: TROPOMI tropospheric NO_2 column averages for (a) 2019, (b) 2020, (c) 2021 and (d) 2022. The averages were calculated using only the days on which MERRA-2 950 hPa winds at 18 UTC were less than 5 ms^{-1}. Pixels with a QA value of less than 0.75 were excluded during the averaging process.

3.3 Hotspots identified by TROPOMI

Aside from analyzing the long-term satellite record of the three areas, we also aimed to assess how well TROPOMI can observe ONG hotspots. The maps in Figure 7a-d show TROPOMI TrC NO_2 averages for each year in 2019-2022. These averages were calculated using only days for the calm wind case (MERRA-2 winds < 5 ms^{-1}) because this yields the best chance at isolating NO_2 hotspots from the surrounding areas. One noticeable difference from year to year is the varying levels of TrC NO_2, both over background and polluted regions. For instance, 2021 had an overall higher background and near shore NO_2 amounts than other years. In 2020, the average offshore amounts were lower, possibly due to restrictions of the COVID-19 pandemic (Bauwens et al., 2021; Fioletov et al., 2022). We identified several hotspots from these maps, shown as an average from mid-2018 through 2022 (Figure 8). The NO_2 hotspots correspond to one or more platforms in the 2017 BOEM emissions inventory.

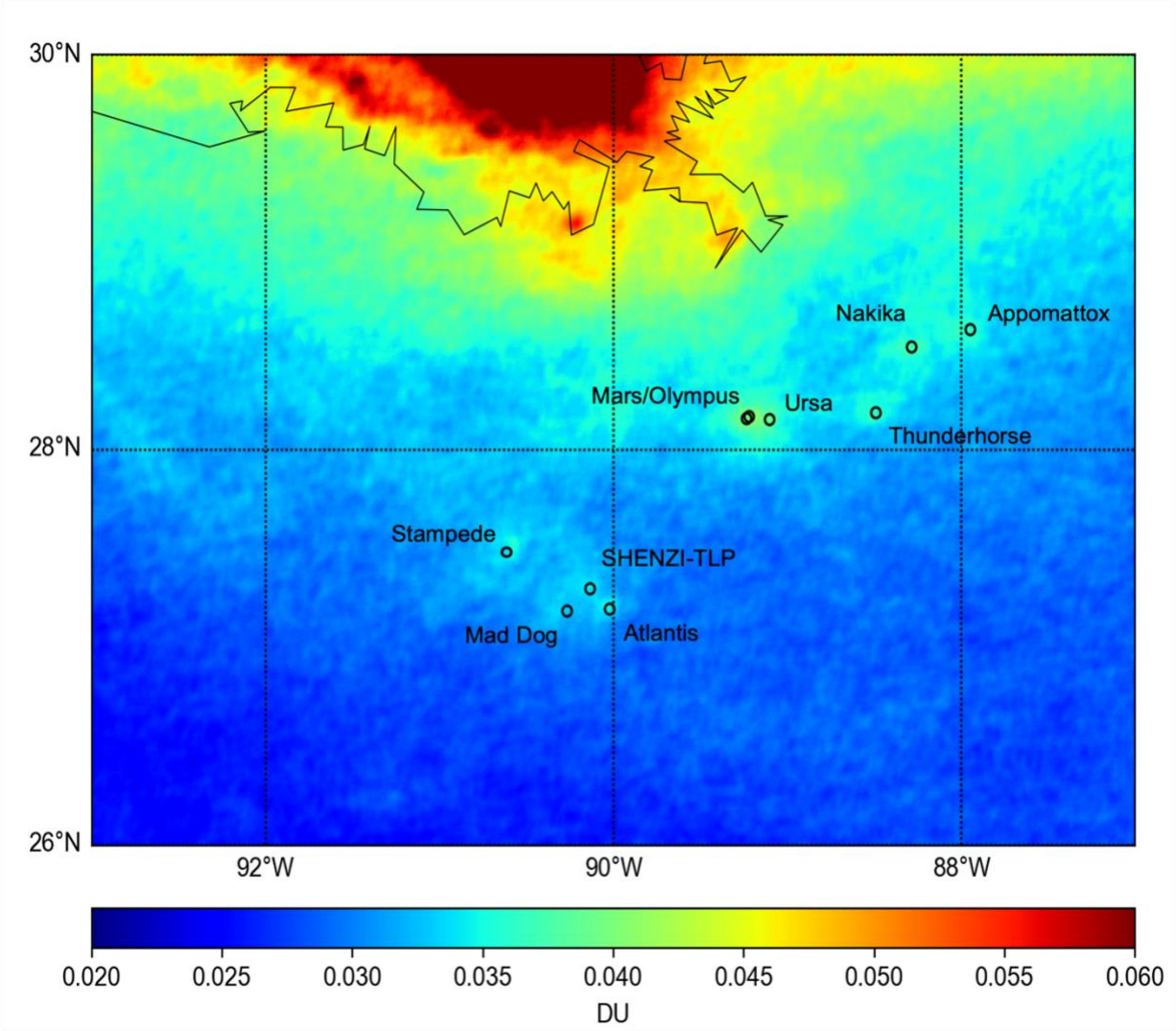

Figure 8: 2018-2022 tropospheric NO_2 column averages from TROPOMI, using only days on which MERRA-2 950 hPa winds at 18 UTC were less than 5 ms^{-1}. The circles and labels show locations of key platforms contributing to the NO_2 column hotspots.

The largest hotspot consists of the Mars and Olympus platforms, both located around 89.22° W and 28.17° N. It is visible clearly in every map in Figure 7. Ursa [89.104° W, 28.154° N], a platform roughly 10 km to the east, also contributes to this hotspot. Other platforms which can be identified are Thunderhorse [88.496° W, 28.19° N], Nakika [88.289° W, 28.521° N], and Appomattox [87.95° W, 28.61° N]. Appomattox only began operations in May 2019, and is visible for every year since 2019. Although located further south in the deepwater region, the Atlantis platform [90.027° W, 27.195° N], in addition to Mad Dog [90.269° W, 27.188° N] and SHENZI-TLP [90.135° W, 27.301° N] platforms all form visible hotspots in the same region on the TROPOMI maps. The hotspot to the northwest of Mad Dog, seen clearly at 90.6° W and 27.5° N is from Stampede, another deepwater platform. It began production in 2018 and so it, like Appomattox, is not included in the BOEM 2017 inventory. The aforementioned platforms are all in the top twenty largest NO_x emitters in the GOM according to the BOEM 2017 inventory, with exception of Stampede and Appomattox, the newer platforms that are not in the inventory. Numerous shallow water platforms are located above 28.5° N closer to the coast;

however, the individual platforms are generally low-NO_x emitters and are more difficult to distinguish from the background NO_2 values in the near-shore area. The Mars/Olympus hotspot represents a 25% increase above background levels of the deepwater area. Other platforms had smaller enhancements: Appomattox, Stampede, Thunderhorse and Atlantis had 13%, 7.7%, 8.1% and 6.9% higher NO_2 than background levels respectively. The hotspot enhancements were calculated by comparing the wind-based time series of each specific hot spot with the deepwater area time series (Figure 9).

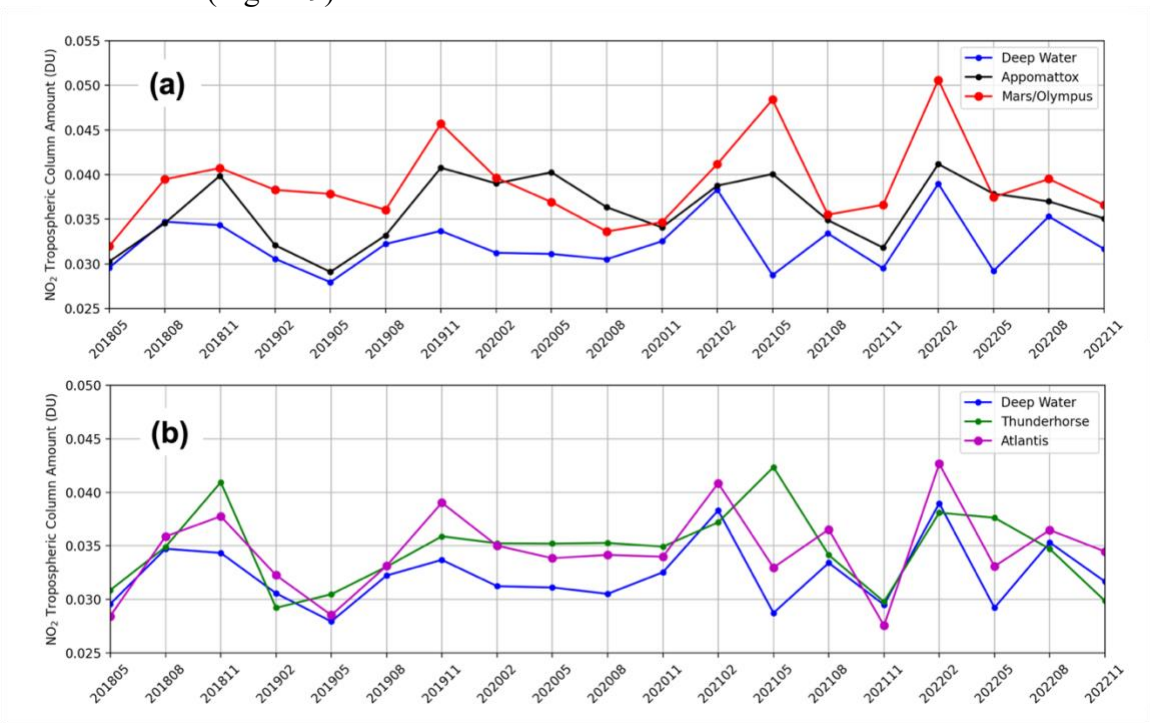

Figure 9: Three-month time series for (a) the Appomattox and Mars/Olympus hotspots compared with the deepwater box (green box in Figure 2), and (b) Atlantis and Thunderhorse hotspots compared with the deepwater box. All of the time series were calculated with the calm wind case evaluated at each respective hotspot.

Time series for the hotspots were calculated with the same method as before, except the TROPOMI pixels used were restricted to within ± 0.1 degrees longitude and latitude of the platform coordinates. Given the distance of deepwater platforms from shore and the NO_2 column amounts being relatively small compared to that of polluted land areas, it is doubtful they produce any significant effects on coastal air quality. For reference, the Mars/Olympus hotspot maximum three-month value is only around 0.05 DU (Figure 9a). Nonetheless, observing these hotspots is important for evaluating the NO_2 budget over the GOM and ultimately validating the NO_x emissions inventories in the future. The NO_2 calm wind anomalies (Figure 10) provide another way to visualize the hotspots. Figure 10 is the average TrC NO_2 percent difference for each 0.01° by 0.01° grid cell between each calm wind day and its respective NO_2 monthly climatology. The same hotspots are visible in the map, the largest of which is Mars/Olympus. The percent anomaly for this hotspot is 9.8%, meaning that calm winds cause the accumulation of an additional 9.8% TrC NO_2 over Mars/Olympus compared to other days. The second and third largest calm wind anomalies are Nakika and Atlantis with 8.5% and 7.8% respectively. A large band of positive NO_2 anomalies stretches across the shallow waters over the area with a

high density of platforms (Figure 10). This is easier to see in the anomaly map rather the overall TROPOMI NO_2 average in Figure 9.

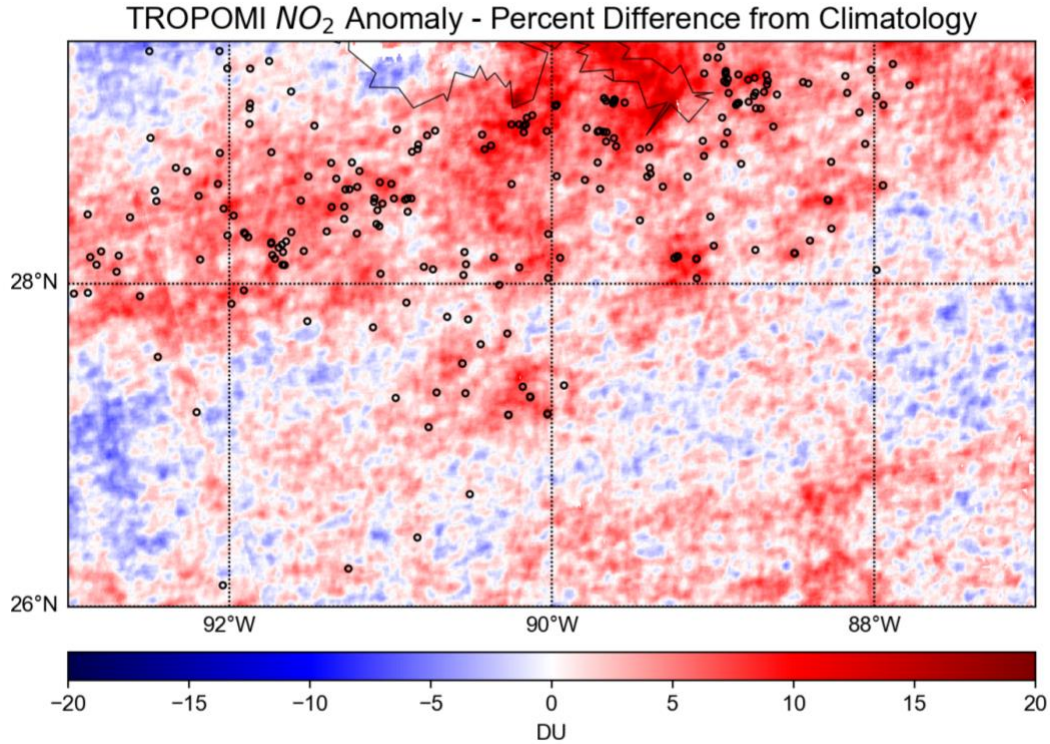

Figure 10: Average TrC NO_2 anomalies from TROPOMI corresponding to calm wind days. The top 250 NO_x emitting platforms from the BOEM 2017 inventory are plotted on the map with empty circles. The TROPOMI data record from May 2018 through December 2022 was used in the calculation and the anomalies were calculated with respect to monthly climatology.

4. Conclusions

We examined the 18+ year record of OMI satellite TrC NO_2 in the GOM region. Three areas were considered for time series analysis: 1) Houston urban, 2) near shore and 3) deep water. A trend analysis on the time series revealed a negative NO_2 trend for the Houston and near shore areas and a slight increasing trend for the deepwater area. The average column amount of the time series for Houston (0.148 DU) was three times greater that of the near shore area (0.0434 DU) which indicates the air over water is clean in comparison, despite the presence of offshore ONG activity. The wind-classified time series showed that ONG activity does have an impact on the NO_2 amount in deepwater region. For instance, in the calm wind case the NO_2 columns were around 33% higher on average than the onshore (wind from the south) case. The calm wind trend for the deepwater area was +0.0021 DU per decade, indicating that there could be a slight increase in NO_x emissions from deepwater ONG platforms since 2005.

We also showed the capability of TROPOMI to observe NO_2 hotspots from oil and natural gas sources in the GOM. On average TROPOMI calm wind case maps, there are clear indications of several NO_2 hotspots in the vicinity of ONG platforms. Visually this is observed mostly in deepwater regions where the background is low enough for the hotspots to be isolated

from the background. The largest hotspot, Mars/Olympus, is 25% above the deepwater background value partly because the two platforms are located only 1.9 km apart. The NO_2 anomalies from monthly climatology during calm wind conditions help quantify relative NO_2 enhancements from ONG operations. Clearly visible are distinct hotspots. Mars/Olympus is the highest, with a 9.8% anomaly for the 2018-2022 TROPOMI record. Positive anomalies are also observed in the shallow water area (north of 28° N) where there are numerous smaller platforms. These platforms, while not clearly identifiable in the TROPOMI NO_2 averages, emit enough NO_x to cause increases above the background values during calm winds.

Given that NO_2 enhancements from emissions can be seen by TROPOMI, a major component of future work will focus on estimating emissions from these hotspots to validate BOEM's ONG NO_x emissions inventories. Liu et al. (2022) and Goldberg et al. 2022) have shown that this can be done without chemical models, using appropriate meteorological data and when a sufficient source signal exists that can be identified in the satellite observations. Presumably their approach can be applied to upcoming data from the TEMPO instrument, which is the first geostationary UV-Vis instrument measuring NO_2 over North America. For validation of TEMPO we will conduct a SCOAPE-II cruise in 2024 with Pandora and in-situ measurements as in Thompson et al. (2023). The work presented here provides the first insight into long-term trends over the GOM and demonstrates the capability of higher-resolution satellite instruments to observe NO_2 hotspots, even over sources with comparatively smaller emissions and spatial footprint than urban areas. Note that TEMPO can monitor ONG emissions as well as mobile marine and land-based NO_x sources hour-by-hour throughout the GOM region. These processes interact throughout the boundary layer NO_2 (Sullivan et al., 2023), contributing to the cycling of reactive nitrogen across a range of environments, e.g., urban business, residential, shipping lanes, ports, the vast petrochemical enterprise and wetlands.

Acknowledgements

This study was partially funded by the U.S. Department of the Interior, Bureau of Ocean Energy Management through Interagency Agreement M23PG00001with NASA (R. Stauffer, PI). Disclaimer: This report has been technically reviewed by BOEM, and it has been approved for publication. The views and conclusions contained in this document are those of the authors and should not be interpreted as representing the opinions or policies of the U.S. Government, nor does mention of trade names or commercial products constitute endorsement or recommendation for use. This research is also supported by an appointment to the NASA Postdoctoral Program at NASA Goddard Space Flight Center, administered by ORAU through a contract with NASA.

Data Availability

OMI total and tropospheric column NO_2 data can be downloaded from NASA GES DISC at https://aura.gesdisc.eosdis.nasa.gov/data/Aura_OMI_Level2/OMNO2.003 (https://doi.org/10.5067/Aura/OMI/ DATA2017; Krotkov et al., 2019). The high resolution OMI dataset is a research data product developed by Lok Lamsal and can be downloaded from: https://avdc.gsfc.nasa.gov/pub/data/satellite/Aura/OMI/V03/L3/OMNO2d_HR/OMNO2d_HRM/ TROPOMI tropospheric NO_2 column data is obtained from the Copernicus Hub at https://scihub.copernicus.eu/ (https:// doi.org/10.5270/S5P-s4ljg54; Copernicus Sentinel-5P, 2019 & 2021). The MERRA-2 data are available from GES DISC at https://disc.gsfc.nasa.gov/datasets/M2I3NPASM_5.12.4/summary (doi:10.5067/QBZ6MG944HW0; GMAO, 2015). All analyses and creation of figures were performed using publicly available Python modules.

References

Bauwens, M., Compernolle, S., Stavrakou, T., Müller, J. F., van Gent, J., Eskes, H., et al. (2020): Impact of coronavirus outbreak on NO_2 pollution assessed using TROPOMI and OMI observations, Geophys. Res. Lett., 47, https://doi.org/10.1029/2020GL087978.

Beirle, S., Platt, U., Wenig, M., & Wagner, T. (2003). Weekly cycle of NO2 by GOME measurements: A signature of anthropogenic sources. *Atmospheric Chemistry and Physics*, 3(6), 2225– 2232. https://doi.org/10.5194/acp-3-2225-2003.

Boersma, K. F., Eskes, H. J., & Brinksma, E. J. (2004). Error analysis for tropospheric NO_2 retrieval from space. *Journal of Geophysical Research,* 109(D4), https://doi.org/10.1029/2003JD003962.

Boersma, K. F., Eskes, H. J., Veefkind, J. P., Brinksma, E. J., van der A, R. J., Sneep, M., Bucsela, E. J. (2007). Near-real time retrieval of tropospheric NO_2 from OMI. *Atmospheric Chemistry and Physics*, 7, 2103– 2118. https://doi.org/10.5194/acp-7-2103-2007.

Burrows, J. P., Weber, M., Buchwitz, M., Rozanov, V., Ladstatter-Weibenmayer, A., Richter, A., et al. (1999). The global ozone monitoring experiment (GOME): Mission concept and first scientific results. *Journal of Atmospheric Sciences*, **56**, 151– 175.

Bell, M. L., Peng, R. D., & Dominici, F. (2006). The exposure-response curve for ozone and risk of mortality and the adequacy of current ozone regulations. *Environmental Health Perspectives*, 114(4), 532– 536. https://doi.org/10.1289/ehp.8816.

Choi, S., Lamsal, L. N., Follette-Cook, M., Joiner, J., Krotkov, N. A., Swartz, W. H., et al. (2020): Assessment of NO_2 observations during DISCOVER-AQ and KORUS-AQ field campaigns, Atmos. Meas. Tech., 13, 2523–2546, https://doi.org/10.5194/amt-13-2523-2020.

Copernicus Sentinel data processed by ESA, Koninklijk Nederlands Meteorologisch Instituut (KNMI) (2019), Sentinel-5P TROPOMI Tropospheric NO2 1-Orbit L2 5.5km x 3.5km, Greenbelt, MD, USA, Goddard Earth Sciences Data and Information Services Center (GES DISC), Accessed: March 2023, https://doi.org/10.5270/S5P-s4ljg54.

Copernicus Sentinel data processed by ESA, Koninklijk Nederlands Meteorologisch Instituut (KNMI) (2021), Sentinel-5P TROPOMI Tropospheric NO2 1-Orbit L2 5.5km x 3.5km, Greenbelt, MD, USA, Goddard Earth Sciences Data and Information Services Center (GES DISC), Accessed: March 2023, https://doi.org/10.5270/S5P-9bnp8q8.

Duncan, B. N. (2020) NASA resources to monitor offshore and coastal air quality. Sterling (VA): U.S. Department of the Interior, Bureau of Ocean Energy Management. OCS Study BOEM 2020-046. 41 p.

Dacic, N., Sullivan, J. T., Knowland, K. E., et al. (2020). Evaluation of NASA's high-resolution global composition simulations: Understanding a pollution event in the Chesapeake Bay during the summer 2017 OWLETS campaign. *Atmospheric Environment*, 222, https://doi.org/10.1016/j.atmosenv.2019.117133.

Fioletov, V., McLinden, C. A., Griffin, D., Krotkov, N., Liu, F., and Eskes, H (2022).: Quantifying urban, industrial, and background changes in NO_2 during the COVID-19 lockdown period based on TROPOMI satellite observations, Atmos. Chem. Phys., 22, 4201–4236, https://doi.org/10.5194/acp-22-4201-2022.

Gelaro, R., McCarty, W., Suárez, M. J., et al. (2017). The Modern-Era Retrospective Analysis for Research and Applications, version 2 (MERRA-2). *Journal of Climate*, **30**(14), 5419– 5454. https://doi.org/10.1175/JCLI-D-16-0758.1

Global Modeling and Assimilation Office (GMAO) (2015), MERRA-2 inst3_3d_asm_Np: 3d,3-Hourly,Instantaneous,Pressure-Level,Assimilation,Assimilated Meteorological Fields V5.12.4, Greenbelt, MD, USA, Goddard Earth Sciences Data and Information Services Center (GES DISC), Accessed: Jan 2023, https://doi.org/10.5067/QBZ6MG944HW0.

Goldberg, D.L.; Anenberg, S.C.; Kerr, G.H.; Mohegh, A.; Lu, Z.; Streets, D.G. (2021): TROPOMI NO_2 in the United States: A detailed look at the annual averages, weekly cycles, effects of temperature, and correlation with surface NO_2 concentrations. *Earth's Futur*, *9*, https://doi.org/10.1029/2020EF001665.

Goldberg, D. L., Harkey, M., de Foy, B., Judd, L., Johnson, J., Yarwood, G., and Holloway, T. (2022): Evaluating NO_x emissions and their effect on O_3 production in Texas using TROPOMI NO_2 and HCHO, Atmos. Chem. Phys., 22, 10875–10900, https://doi.org/10.5194/acp-22-10875-2022.

Herman, J., Cede, A., Spinei, E., et al. (2009): NO_2 column amounts from ground-based Pandora and MFDOAS spectrometers using the direct-sun DOAS technique: Intercomparisons and application to OMI validation, J. Geophys. Res., 114, D13307, https://doi.org/10.1029/2009JD011848.

Jensen, M. P., Flynn, J. H., Judd, L. M., Kollias, P., Kuang, C., Mcfarquhar, G., et al. (2022). A succession of cloud, precipitation, aerosol, and air quality field experiments in the coastal urban environment. Bulletin of the American Meteorological Society, 103(2), 103– 105. https://doi.org/10.1175/bams-d-21-0104.1.

Judd, L. M., Al-Saadi, J. A., Janz, S. J, et al. (2019): Evaluating the impact of spatial resolution on tropospheric NO_2 column comparisons within urban areas using high-resolution airborne data, Atmos. Meas. Tech., 12, 6091–6111, https://doi.org/10.5194/amt-12-6091-2019.

Judd, L. M., Sullivan, J. T., Lefer, B., Haynes, J., Jensen, M. P., & Nadkarni, R. (2021). TRACER-AQ science plan: An interagency cooperative air quality field study in the Houston, TX Metropolitan Region. Retrieved from https://www-air.larc.nasa.gov/missions/tracer-aq/docs/TRACERAQ_SciencePlan_v1.pdf

Kollonige, D. E., Thompson, A. M., Josipovic, M., et al. (2018). OMI satellite and ground-based Pandora observations and their application to surface NO_2 estimations at terrestrial and marine sites. J. Geophys. Res., 123, 1441-1459, https://doi.org/10.1002/2017JD026518.

Kotsakis, A., Sullivan, J. T., Hanisco, T. F., Swap, R. J., Caicedo, V., Berkoff, T. A., et al. (2022). Sensitivity of total column NO_2 at a marine site within the Chesapeake Bay during OWLETS-2. *Atmospheric Environment*, 277, 119063. https://doi.org/10.1016/j.atmosenv.2022.119063

Levelt, P., Van den Oord, G., Dobber, M., et al. (2006). The ozone monitoring instrument, IEEE Transactions on Geosci, and Remote Sensing*, 44*(5), 1093-1101.

Levelt, P. F., Joiner, J., Tamminen, J., et al. (2018) The ozone monitoring instrument: Overview of 14 years in space, Atmospheric Chemistry and Physics, 18(8):5699–5745, https://doi.org/10.5194/acp-18-5699-2018.

Lamsal, L. N., Duncan, B. N., Yoshida, Y., Krotkov, N. A., Pickering, K. E., Streets, D. G., & Lu, Z. (2015). U.S. NO_2 trends (2005–2013): EPA air quality system (AQS) data versus improved observations from the ozone monitoring instrument (OMI). *Atmospheric Environment*, 110, 130– 143. https://doi.org/10.1016/j.atmosenv.2015.03.055.

Lamsal, L. N., Krotkov, N. A., Vasilkov, A., et al. (2021): Ozone Monitoring Instrument (OMI) Aura nitrogen dioxide standard product version 4.0 with improved surface and cloud treatments, Atmos. Meas. Tech., 14, 455–479, https://doi.org/10.5194/amt-14-455-2021.

Liu, F., Tao, Z., Beirle, et al. (2022): A new method for inferring city emissions and lifetimes of nitrogen oxides from high-resolution nitrogen dioxide observations: a model study, Atmos. Chem. Phys., 22, 1333–1349, https://doi.org/10.5194/acp-22-1333-2022.

Krotkov, N. A., McLinden, C. A., Li, C., Lamsal, L. N., Celarier, E. A., Marchenko, S. V., Swartz, W. H, et al. (2016): Aura OMI observations of regional SO_2 and NO_2 pollution changes from 2005 to 2015, Atmos. Chem. Phys., 16, 4605–4629, https://doi.org/10.5194/acp-16-4605-2016.

Krotkov, N. A., Lamsal, L. N., Marchenko, S. V., Bucsela, E. J., Swartz, W. H., & Joiner, J., & The OMI Core Team. (2019). OMI/Aura nitrogen dioxide (NO2) total and tropospheric column 1-orbit L2 swath 13x24 km V003. Goddard Earth Sciences Data and Information Services Center (GES DISC). Accessed Sept. 2022. https://doi.org/10.5067/Aura/OMI/DATA2017

Martins, D. K., Najjar, R. G., Tzortziou, M., Abuhassan, N., Thompson, A. M., & Kollonige, D. E. (2016). Spatial and temporal variability of ground and satellite column measurements of NO_2 and O_3 over the Atlantic Ocean during the deposition of atmospheric nitrogen to coastal ecosystems experiment (DANCE). *Journal of Geophysical Research*, 121(23), 14,175– 14,187. https://doi.org/10.1002/2016JD024998

Munro, R., Lang, R., Klaes, D., Poli, G., Retscher, C., Lindstrot, R., et al. (2016): The GOME-2 instrument on the Metop series of satellites: instrument design, calibration, and level 1 data processing – an overview, Atmos. Meas. Tech., 9, 1279–1301, https://doi.org/10.5194/amt-9-1279-2016.

Nowlan, C. R., Liu, X., Leitch, J. W. (2016): Nitrogen dioxide observations from the Geostationary Trace gas and Aerosol Sensor Optimization (GeoTASO) airborne instrument: Retrieval algorithm and measurements during DISCOVER-AQ Texas 2013, *Atmospheric Measurement Techniques,* 9, 2647–2668, https://doi.org/10.5194/amt-9-2647-2016.

Nowlan, C. R., Liu, X., Janz, S. J., Kowalewski, M. G., Chance, K., Follette-Cook, M. B., et al. (2018): Nitrogen dioxide and formaldehyde measurements from the GEOstationary Coastal and Air Pollution Events (GEO-CAPE) Airborne Simulator over Houston, Texas, Atmos. Meas. Tech., 11, 5941–5964, https://doi.org/10.5194/amt-11-5941-2018.

Piters, A. J. M., Boersma, K. F., Kroon, M., Hains, J. C., Van Roozendael, M., Wittrock, F., Abuhassan, N, et al. (2012): The Cabauw Intercomparison campaign for Nitrogen Dioxide measuring Instruments (CINDI): design, execution, and early results, Atmos. Meas. Tech., 5, 457–485, https://doi.org/10.5194/amt-5-457-2012.

Reed, A. J., Thompson, A. M., Kollonige, D. E., Martins, D. K., Tzortziou, M. A., Herman, J. R., et al. (2015): Effects of local meteorology and aerosols on ozone and nitrogen dioxide retrievals from OMI and pandora spectrometers in Maryland, USA during DISCOVER-AQ 2011, *J. Atmos. Chem*., 72, 455–482, https://doi.org/10.1007/s10874-013-9254-9.

Richter, A., & Burrows, J. P. (2002). Tropospheric NO2 from GOME measurements. *Advances in Space Research*, 29, 1673– 1683, https://doi.org/10.1016/S0273-1177(02)00100-X.

Richter, A., Begoin, M., Hilboll, A., and Burrows, J. P. (2011): An improved NO_2 retrieval for the GOME-2 satellite instrument, Atmos. Meas. Tech., 4, 1147–1159, https://doi.org/10.5194/amt-4-1147-2011.

Shah, V., Jacob, D. J., Li, K., Silvern, R. F., Zhai, S., Liu, M., et al. (2020). Effect of changing NOx lifetime on the seasonality and long-term trends of satellite-observed tropospheric NO_2 columns over China. *Atmospheric Chemistry and Physics Discussions*, 20(3), 1483–1495. https://doi.org/10.5194/acp-2019-670.

Sullivan, J. T., Berkoff, T., Gronoff, G., et al. (2018): The ozone water-land environmental transition study (OWLETS): An innovative strategy for understanding Chesapeake Bay pollution events. Bulletin of the American Meteorological Society. https://doi.org/10.1175/BAMS-D-18-0025.

Sullivan, J., Dreessen, T., Berkoff, T., et al. (2020) An overview of NASA's Ozone Water–Land Environmental Transition Study (OWLETS) of the Chesapeake Bay airshed. EM Magazine (Air and Waste Management Assn), October 2020.

Sullivan, J. T., Stauffer, R. M., Thompson, A. M., Tzortziou, M. A., Loughner, C. P., Jordan, C. E., & Santanello, J. A. (2023). Surf, turf, and above the Earth: Unmet needs for coastal air quality science in the planetary boundary layer (PBL). *Earth's Future*, 11, e2023EF003535. https://doi.org/10.1029/2023EF003535

Thompson, A. M., Stauffer, R. M., Boyle, T. P, et al. (2019): Comparison of near-surface NO2 pollution with Pandora total column NO_2 during the Korea-United States Ocean Color (KORUS OC) campaign, 2019, Journal of Geophysical Research: Atmospheres, 124, https://doi.org/10.1029/2019JD030765.

Thompson, A .M., Kollonige, D. E., Stauffer, R.M., et al. (2020): Satellite and shipboard views of air quality along the Louisiana coast: The 2019 SCOAPE (Satellite Coastal and Oceanic Atmospheric Pollution Experiment) cruise, EM Magazine (Air and Waste Management Assn), Oct 2020.

Thompson, A.M., Kollonige, D.E., Stauffer, R.M., et al. (2023): Two air quality regimes in total column NO_2 over the Gulf of Mexico in May 2019: Shipboard and satellite views, Earth and Space Science, https://doi.org/10.1029/2022EA002473Torres, O., Bhartia, P. K., Jethva, H., and Ahn, C. (2018): Impact of the ozone monitoring instrument row anomaly on the long-term record of aerosol products, Atmos. Meas. Tech., 11, 2701–2715, https://doi.org/10.5194/amt-11-2701-2018.

Torres, O., Bhartia, P. K., Jethva, H., and Ahn, C. (2018): Impact of the ozone monitoring instrument row anomaly on the long-term record of aerosol products, Atmos. Meas. Tech., 11, 2701–2715, https://doi.org/10.5194/amt-11-2701-2018.

Tzortziou, M., Herman, J., Cede, A., Loughner, C., Abuhassan, N., Naik, S. (2013): Spatial and temporal variability of ozone and nitrogen dioxide over a major urban estuarine ecosystem. *J. Atmos. Chem.*, 72. https://doi.org/10.1007/s10874-013-9255-8.

Tzortziou, M., Parker, O., Lamb, B., et al. (2018): Atmospheric trace gas (NO_2 and O_3) variability in Korean coastal waters, implications for remote sensing of coastal ocean color dynamics, *Remote Sens.*, 2018, *10,* 1587; https://doi.org/10.3390/rs10101587.

Veefkind, J., Aben, I., McMullan, K., et al. (2012). TROPOMI on the ESA Sentinel-5 Precursor: A GMES mission for global observations of the atmospheric composition for climate, air quality and ozone layer applications. Remote Sens. of Environ., 120, 70–83, https://doi.org/10.1016/j.rse.2011.09.027.

van Geffen, J. H., Eskes, H. J., Boersma, K. F., et al. (2018). TROPOMI ATBD of the total and tropospheric NO_2 data products (issue 1.2.0). Royal Netherlands Meteorological Institute (KNMI), De Bilt, the Netherlands, s5P-KNMI-L2-0005-RP.

van Geffen, J. H., Boersma, K. F., Eskes, H., Sneep, M., ter Linden, M., Zara, M., & Veefkind, J. P. (2020). S5P TROPOMI NO slant column retrieval: method, stability, uncertainties and comparisons with OMI. *Atmospheric Measurement Techniques*, **13**(3), 1315– 1335. https://doi.org/10.5194/amt-13-1315-2020.

Wilson, D., Enoch, S., Mendenhall, S., et al. (2018): User's guide for the 2017 Gulfwide Offshore Activities Data System (GOADS-2017). New Orleans (LA): U.S. Dept. of the

Interior, Bureau of Ocean Energy Management, Gulf of Mexico OCS Region. OCS Study BOEM 2018-038.

Satellite NO_2 Trends and Hotspots over Offshore Oil and Gas Operations in the Gulf of Mexico

Niko M. Fedkin[1,3], Ryan M. Stauffer[1], Anne M. Thompson[1,2], Debra E. Kollonige[1,3] , Holli D. Wecht[4], Nellie Elguindi[4]

[1]Earth Sciences Division, NASA/Goddard Space Flight Center, Greenbelt, MD, USA
[2] GESTAR and Joint Center for Earth Systems Technology, University of Maryland, Baltimore County, Baltimore, MD, USA
[3] SSAI., Lanham, MD, USA
[4]Bureau of Ocean Energy Management, Office of Environmental Programs, Sterling, VA, USA

Corresponding author: Niko Fedkin (niko.m.fedkin@nasa.gov)

Key Points:

- Satellite NO_2 records and trends of urban, coastal and deep water areas from 2005 to 2022, are presented
- Classifying NO_2 over the Gulf of Mexico (GOM) under various wind conditions highlights typical patterns in average NO_2 values
- GOM NO_2 hotspots from deepwater platforms were identified by TROPOMI under calm wind conditions, the largest of which is over Mars/Olympus

Abstract

The Outer Continental Shelf of the Gulf of Mexico (GOM) is populated with numerous oil and natural gas (ONG) platforms which produce NO_x ($NO_x = NO + NO_2$), a major component of air pollution. The Bureau of Ocean Energy Management (BOEM) is mandated to ensure that the air quality of coastal states is not degraded by these emissions. As part of a NASA-BOEM collaboration, we conducted a satellite data-based analysis of nitrogen dioxide (NO_2) patterns and trends in the GOM. Data from the OMI and TROPOMI sensors were used to obtain 18+ year records of tropospheric column (TrC) NO_2 in three GOM regions: 1) Houston urban area, 2) near shore area off the Louisiana coast, and a 3) deepwater area off the Louisiana coast. The 2004-2022 time series show a decreasing trend for the urban (-0.027 DU/decade) and near shore (-0.0022 DU/decade) areas, and an increasing trend (0.0019 DU/decade) for the deepwater area. MERRA-2 wind and TROPOMI NO_2 data were used to reveal several NO_2 hotspots (up to 25% above background values) under calm wind conditions near individual platforms. The NO_2 signals from these deepwater platforms and the high density of shallow water platforms closer to shore were confirmed by TrC NO_2 anomalies of up to 10%, taking into account the monthly TrC NO_2 climatology over the GOM. The results presented in this study establish a baseline for future estimates of emissions from the ONG hotspots and provide a methodology for analyzing NO_2 measurements from the new geostationary TEMPO instrument.

Plain Language Summary

Oil and natural gas operations emit nitrogen oxides (NO_x), which are major air pollutants and precursors to ground-level ozone. The Bureau of Ocean Energy Management (BOEM) agency is responsible for managing planned oil and natural gas (ONG) activity on the outer continental

shelf, and is mandated to ensure related emissions do not degrade air quality of coastal states. In collaboration with BOEM, we used satellite data from the OMI and TROPOMI sensors to construct an 18+ year record of tropospheric nitrogen dioxide (NO_2), a proxy for NO_x, in the Gulf Coast region. These time series focused on three areas: 1) Houston urban, 2) off the Louisiana coast, and 3) deepwater Gulf off Louisiana. These regions experienced changes in tropospheric column NO_2 of -13.7%, -5.8% and +5.4% per decade, respectively. We also identified NO_2 hotspots from ONG platforms using TROPOMI NO_2 averages under calm wind conditions. The ONG deepwater platforms enhance NO_2 background amounts by 7-13% on average, and up to 25% for the Mars and Olympus platforms combined. The results presented here will facilitate our work on emissions estimates from these sources and on applications to the recently launched TEMPO instrument.

1. Introduction

Nitrogen dioxide (NO_2), a component of NO_x ($NO_x = NO + NO_2$) and classified as a criterion pollutant by the Environmental Protection Agency (EPA), is produced from fuel combustion. Anthropogenic sources of NO_2 include fires, vehicular emissions, power plants and other industrial activities such as oil and natural gas (ONG) production. In large quantities, NO_2 causes respiratory problems from prolonged exposure. Furthermore, NO_2 is a major precursor to tropospheric ozone (O_3), another criteria pollutant responsible for damaging effects on lungs and premature mortality (Bell et al., 2006). Amounts of NO_2 are measured with in-situ analyzers, typically reporting in mixing ratio, or through remote sensing instruments that report column amounts. Ground-based remote sensors for total column NO_2 (TC NO_2, Piters et al., 2012) include the Pandora spectrometer (Herman et al., 2009). Airborne remote sensors, e.g., the Geo-CAPE Airborne Simulator (GCAS) (Nowlan et al., 2018; Judd et al., 2019) and the Geostationary Trace gas and Aerosol Sensor Optimization (GEO-TASO) (Nowlan et al., 2016) measure the NO_2 column amount below the aircraft. From space, TC NO_2 is measured with satellite ultraviolet-visible (UV-Vis) sensors. A long TC NO_2 record exists thanks to a series of satellite sensors: the Global Ozone Monitoring Experiment (GOME, Burrows et al., 1999; Richter et al., 2002) and GOME-2 (Richter et al., 2011; Munro et al., 2016) instruments, the Ozone Monitoring Instrument (OMI) (Levelt et al., 2006; Levelt et al., 2018), and the Tropospheric Monitoring Instrument (TROPOMI) instrument launched in 2017 (Van Geffen et al., 2012). TROPOMI also supplies a tropospheric column (TrC) NO_2 product, which has been used for a range of air quality applications.

Satellite instruments are very useful for providing column NO_2 data over areas without surface monitoring, especially over water. Over the past decade a number of studies have compared satellite TC NO_2 with both in-situ and remotely sensed NO_2 in coastal areas. Land-sea interactions, e.g., sea-breeze and other dynamical factors, show how challenging satellite NO_2 validation can be over both sides of the land-water interface. The Korea-United States Ocean Color experiment (KORUS-OC) (Tzortziou et al., 2018; Thompson et al., 2019), around the Korean Peninsula in 2016, found that complex interactions of advected pollution and meteorology determined whether satellite TC NO_2 column amounts correlated with shipboard Pandora TC NO_2 and in-situ NO_2 measurements. Similarly, the Ozone Water-Land Environmental Transition Study (OWLETS) projects over the southern Chesapeake Bay region in 2017 (Sullivan et al., 2018; Dacic et al., 2020) and near Baltimore in 2018 (Sullivan et al., 2020; Kotsakis et al., 2022) discovered that the accuracy of satellite TC NO_2 data depended on resolution (pixel size), cloud-cover, pollution amount and whether the satellite was measuring

over land or water. Other campaigns with TC NO_2 measurements in coastal areas include DISCOVER-AQ in Baltimore (2011) (Ttzortiou et al., 2013; Reed et al., 2015) and Houston (2013) (Judd et al., 2019; Choi et al., 2020), and the Deposition of Atmospheric Nitrogen to Coastal Ecosystems (DANCE) campaign in (Martins et al., 2016; Kollonige et al., 2019).

In the Gulf of Mexico (GOM), a notable source of NO_x is from ONG exploration and production sites. The above-mentioned campaigns, while investigating air quality in coastal regions, did not focus on areas of concentrated offshore ONG activity or validation of satellite NO_2 near ONG sources. We addressed these issues in a 3-year study that NASA undertook in collaboration with the Bureau of Ocean Energy Management (BOEM, Department of Interior). BOEM is the agency responsible for managing ONG exploration, development, and production plans in the U.S. Outer Continental Shelf (OCS). The agency specifically has air quality jurisdiction for OCS emissions from ONG exploration and development to the west of 87.5°. It is also mandated to ensure that criteria pollutant emissions from these activities are in compliance with the national ambient air standards to the extent that the activities do not significantly affect the air quality of any state. BOEM tracks industry-reported NO_x emissions from ONG operations in monthly inventories (Wilson et al., 2018). However, due to lack of air quality monitoring on the OCS, the reported emissions remain unvalidated. NASA and BOEM carried out a feasibility study from 2017 to 2020 to determine whether satellite data could be used to monitor NO_2 over the GOM and discriminate regional sources and/or resolve pollution from individual platforms. Preliminary results were summarized in two documents by Duncan (2020) and Thompson (2020). These were followed by detailed reports on a 2019 field campaign (Satellite Coastal and Oceanic Atmospheric Pollution Experiment), SCOAPE-I (Thompson, 2020; Thompson et al., 2023), along the Louisiana coast.

The SCOAPE-I cruise took place 10-18 May 2019 aboard the *Research Vessel Point Sur*. One of the goals of this campaign was to measure in-situ NO_2 levels along the Louisiana coast with a cruise track designed to sample smaller near-shore ONG operations, over open water, and near large deepwater ONG platforms farther away from the coast. The deepwater platforms primarily produce oil and flare excess gas; thus, they usually have larger individual platform NO_x emissions. For NO_2, the *Point Sur* was equipped with a NO_2 in-situ analyzer and a Pandora spectrometer for measuring TC NO_2 amounts. Pandora measurements were taken during daytime in cloud-free conditions. Measurements of NO_2 were also collected with Pandora, satellites, and an NO_2 analyzer at the Louisiana Universities Marine Consortium (LUMCON; Cocodrie, LA; 29.26°, 90.66°) SCOAPE-I port during the cruise and the three weeks prior.

During the SCOAPE I cruise, satellite (OMI, TROPOMI) and the shipboard Pandora total column (TC) NO_2 levels were elevated in the vicinity of ONG platforms as confirmed by numerous coincident NO_2 spikes from the shipboard analyzer. However, neither the satellite nor Pandora TC NO_2 responses to emissions were as large as surface NO_2 increases. Comparisons between NO_2 column amounts from satellite and surface Pandoras showed good agreement during SCOAPE I - within 13% over water and 5% over land in clear sky conditions - and NO_2 signals from selected ONG platforms could sometimes be isolated (Thompson et al., 2023). However, consistent quantification of NO_2 sources was not possible due to cloud cover, satellite sampling frequency (one overpass daily) and relatively coarse spatial resolution compared to platform size, factors all amplified by the short duration of the cruise. Two air quality regimes, differentiated by prevailing wind direction, were characterized by surface and satellite measurements during SCOAPE I: clean marine air over deepwater (onshore wind from remote marine locations) and polluted continental air near shore (wind from land). In between, elevated NO_2 near-shore can result from nearby pollution, from deepwater regions <u>*or*</u> from the continent.

There is now nearly five years of TROPOMI and 18+ years of OMI observations, both TC NO_2 and TrC NO_2. This prompts us to conduct a more comprehensive study of satellite NO_2 over the GOM, examining regional and temporal variability. We use OMI and TROPOMI TrC NO_2 data to: 1) analyze the long-term NO_2 record over three prototype regions within the GOM and 2) identify NO_2 hotspots near ONG operations using wind-classified TROPOMI data. The longer time-series are used to determine trends in NO_2. Anomalous calm-wind TROPOMI data pinpoint major and lesser-emitting platforms. The results, summarized in Section 3.1 and 3.2, provide a baseline for the longer-term goal of monitoring GOM ONG NO_x emissions. Identifying the hotspots is crucial for BOEM's mission and demonstrates the ability to monitor ONG pollution with remote sensing instruments in anticipation of the geostationary Tropospheric Emissions: Monitoring of Pollution (TEMPO) data. The results for this second objective are found in Section 3.3.

2. Methodology

2.1 Description of study domain

The focus area is the Outer Continental Shelf (OCS) of the Gulf of Mexico (GOM), an area populated with numerous oil and natural gas platform operations (Figure 1). There are two main types of platforms: shallow water and deepwater platforms. Deepwater platforms are further from the coast, more isolated, and produce NO_x emissions due to gas flaring. Shallow water platforms generally produce less NO_x than deepwater platforms but are greater in density near the shore. The majority of the platforms in the GOM produce less than 1000 metric tons of NO_2 per year with exception of the deepwater platforms away from shore, according to the 2017 BOEM inventory (Figure 1; Wilson et al., 2018). The domain of this study is between 25°N and 30° N latitude and 95° W and 87.5° W longitude. This includes most of the OCS of the GOM over which BOEM has jurisdiction (200 nautical miles beyond state jurisdictions). We also consider the Houston, TX, urban area as a reference in comparison to the areas over water. In particular, Houston was chosen because it is the highest NO_x emitting region along the Gulf coast and has been the location of multiple air quality campaigns such as DISCOVER-AQ (Judd et al., 2019; Nowlan et al., 2018; Choi et al., 2020) and TRACER-AQ in 2021 (Jensen et al., 2022; Judd et al., 2021).

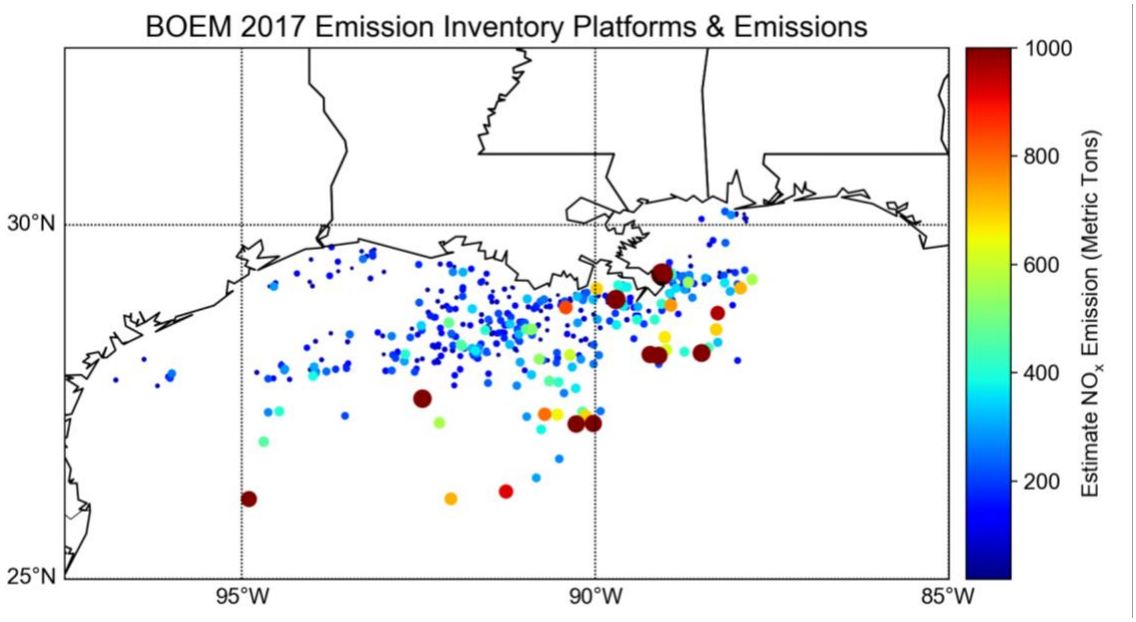

Figure 1: Locations of the Gulf of Mexico ONG platforms in the BOEM 2017 emission inventory. Larger dots and corresponding colors indicate the platforms with the highest annual NO_x emissions.

The study domain was further divided into smaller regions to compare areas that are expected to have contrasting NO_x emissions and observed NO_2 amounts. A deepwater area, a near shore area and an urban area were defined and shown as a green, red and orange box in Figure 2, respectively. The near shore area covers parts of both BOEM (federal) and Louisiana state jurisdictions, and includes numerous shallow water platforms within about 100 km from the Louisiana coast. The latitude bound of the near shore area is 28.3° N and 29.3° N in this analysis. The defined deepwater area is between 27° and 28.3° N and includes several deepwater operations with NO_x emissions greater than 500 metric tons. In this study, the deepwater area can also be treated as being close to background NO_2 levels, since marine air is clean and the deepwater platforms are relatively isolated.

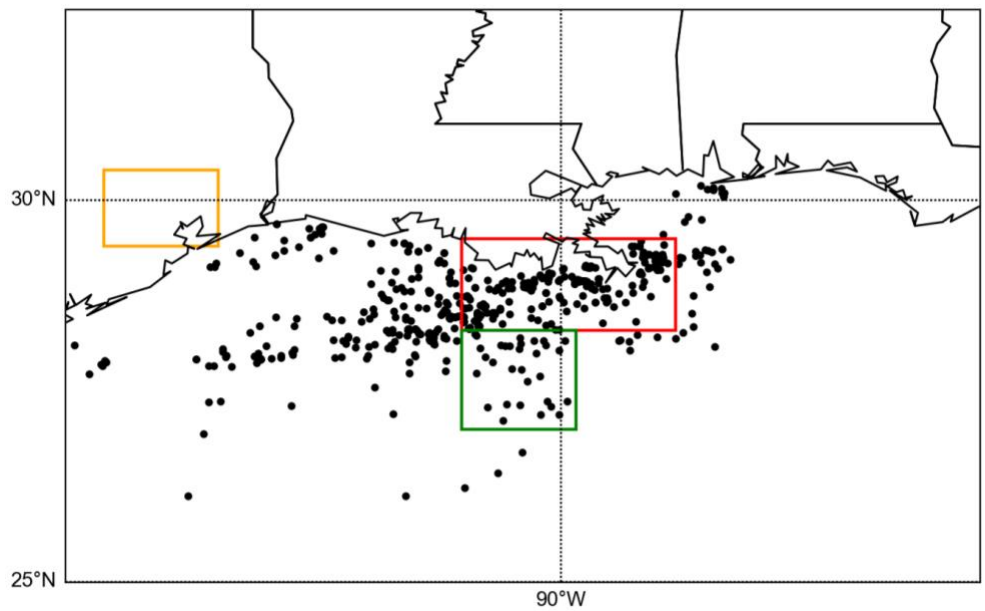

Figure 2: Map of the three areas of focus for which OMI and TROPOMI time series are calculated: Shallow water off the east Louisiana coast (red box), GOM deepwater (green box) and Houston, TX, metropolitan area (orange box). Each black dot represents a platform or facility in the BOEM OCS 2017 emissions inventory.

2.2 Datasets

For this work, we used satellite datasets from the Ozone Monitoring Instrument (OMI) (Levelt et al., 2006; Levelt et al., 2018) and TROPOMI (Veefkind et al., 2012). Located onboard NASA's polar orbiting Aura satellite, OMI was launched in 2004 and its data record began in October of that year. OMI collects observations over a particular location about once a day at a spatial resolution of 13 x 24 km^2 at nadir and 24x160 km^2 at the edge of the swath. The satellite is sun synchronous and makes an overpass at around 1300-1400 local time. In this study we use the high-resolution OMI Tropospheric NO_2 Version 4 dataset (Lamsal et al., 2021; https://avdc.gsfc.nasa.gov/pub/data/satellite/Aura/OMI/V03/L3/OMNO2d_HR), which contains several improvements to air mass factors (AMFs) compared to Version 3. In particular, this version incorporates improved cloud algorithms, a geometric Lambertian Equivalent Reflectance (GLER) product and improved terrain pressure calculations into the NO_2 retrieval. This Level 3 (L3) gridded research product has a resolution of 0.1° × 0.1° – an increase from the 0.25° × 0.25° of the original Level 3 dataset. At times the spatial coverage of OMI is impacted by the row anomaly (Torres et al., 2018), a physical instrument issue which obstructs some of the instrument's field of view and therefore affects radiance measurements.

The TROPOMI instrument was launched by the European Space Agency on the European Union's Copernicus Sentinel 5 Precursor (S5P) satellite in October 2017, with the data record beginning May 2018. The overpass of TROPOMI occurs in early afternoon, within about 0.5 hr. of OMI. The resolution of the instrument is currently 3.5 × 5.6 km^2 at nadir (3.5 × 7 km^2 prior to August 2019). Like other polar orbiting instruments, TROPOMI provides daily global coverage, although only about once per day at any given location. TROPOMI's NO_2 algorithms use a differential optical absorption spectroscopy (DOAS) technique on radiances in the 405–465 nm spectral window. The spectral radiances are converted into slant column

densities (SCD) of NO_2 between the instrument and the Earth's surface (van Geffen et al., 2020). AMFs are then used to convert the slant column into a vertical column density (VCD). For obtaining the tropospheric NO_2 column, the stratospheric portion is subtracted from the total SCD using global model estimates (Boersma et al., 2004; Boersma et al., 2007). The algorithms have been updated throughout the course of TROPOMI's operation, resulting in multiple versions of the data. The research dataset S5P-PAL (https://data-portal.s5p-pal.com/products/no2) was developed to apply the new algorithm (v2.3) to the older radiances, essentially homogenizing the data with respect to retrieval differences.

Lastly, we use the Modern Era Retrospective Analysis for Research and Applications Version 2 (MERRA-2, Gelaro et al., 2017) for wind analysis incorporated into calculating the satellite NO_2 time series. MERRA-2 is derived from the GEOS-5 data assimilation system and contains meteorological variables on a 0.5°× 0.625° grid for 42 standard pressure levels. The variables used in the analysis are the U and V components of the wind which are used to derive vector wind speed and direction.

2.3 Satellite NO_2 Time Series

The time series in this work consist of monthly averages of TrC NO_2. For OMI, a monthly version of the L3 high-resolution dataset is already available as a research product. The TROPOMI data were compiled by finding all overpasses over our study region in that month, re-gridding each daily file to a 0.01° × 0.01° grid and calculating the average for each grid point. The recommended quality assurance (QA) value of 0.75 was used as a threshold for filtering bad quality pixels. Next, the grid cells in each area previously described (deepwater, near shore and urban) were averaged for each month to obtain the time series for that particular region. From the resulting time series of monthly averages we also calculated the 12 month moving averages to account for the seasonality in the NO_2 time series. A trend line was fitted to the moving average to obtain an overall linear trend over the full record. The trends are presented in Section 3 along with the 95% confidence intervals.

Since meteorological regimes drove much of the variability in TC NO_2 in coastal areas during SCOAPE-I (Thompson et al., 2023), we also analyzed how the time series differ according to different wind speed and directions (source regions). For this objective, daily MERRA-2 wind data from 2005-2022 were used to restrict the NO_2 averaging to days based on three cases: 1) Wind from the north (land) at greater than 10 ms^{-1} 2) wind from the south (GOM) at greater than 10 ms^{-1} and 3) calm winds of less than 5 ms^{-1}. The 10 ms^{-1} threshold was chosen to ensure that sufficient transport was occurring that day within the lower levels of the atmosphere. For the north and south wind conditions, we defined the degree bounds as 120° to 240° and 300° to 60°, respectively. Note that here we use meteorological wind directions where due north is 360°. For the calm wind case, all wind directions are considered. It is important to note that 140-160 days out of the year are ignored, such as those with wind speeds between 5 and 10 ms^{-1}. For the Houston, TX box, the wind direction bounds were rotated by 45° counterclockwise in order to account for orientation of land and sea with respect to the city. The overall objective of this analysis was to determine how much the NO_2 column amount averages differ based on land vs. marine source regions, as well as cases with calm conditions and less regional transport. The MERRA-2 winds were evaluated for all MERRA-2 grid points within each box in Figure 2. A specific day was categorized if the wind direction was within the degree bounds and wind speed condition was met at all points. The 950 hPa pressure level was used because we are generally interested in the wind in the boundary layer but not specifically at the surface in the case that there is transport occurring aloft. The model surface winds also tend to

carry more uncertainty than at levels aloft. To best coincide with the overpass of OMI and TROPOMI, we only used the wind information at 18 UTC (12-1 pm local time).

Once the sets of days corresponding to each wind criterion were compiled, 3-month averages were computed from those days for each NO_2 time series. Three-month periods were used to account for sample size issues; some months have too few days of a wind criterion being met. For example, calm winds are more common in the summer than winter according to the climatology compiled from the MERRA-2 data (Figure 3). Aside from using the selected days for each case, the procedure for averaging the TROPOMI Level 2 (L2) and OMI L3 gridded data files was the same. This analysis yielded three time series for each area, corresponding to the three wind criteria. These results and their implications are discussed in Section 3.

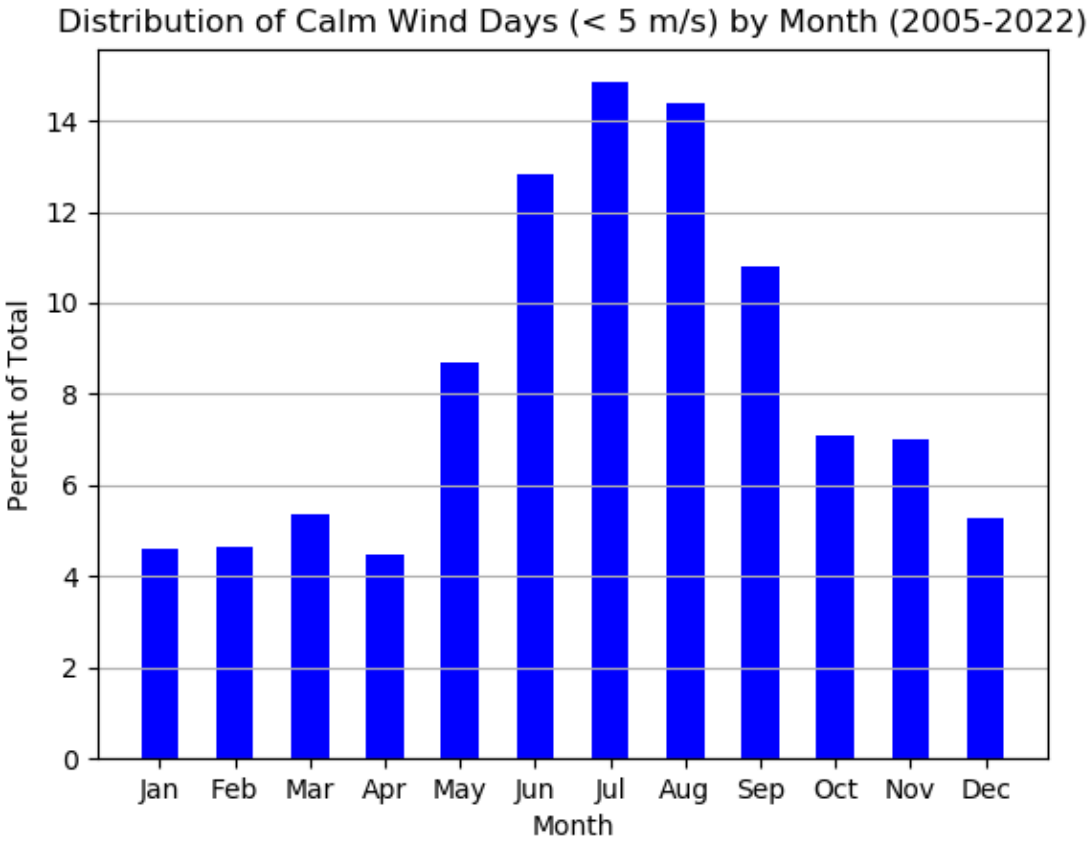

Figure 3: Distribution of number of days for each month for which the MERRA-2 950 hPa wind evaluated in the near shore area was less than 5 ms^{-1} (calm wind case). It is expressed as a percentage of the total number of days over the 18 years of the OMI record (2005 through 2022).

2.4 TROPOMI NO_2 Averages and Anomalies

The wind-based averaging was extended to TROPOMI data, with the goal of identifying NO_2 hotspots. This was done on an annual basis by calculating an average of all days in each year that fit the calm wind case (winds < 5 ms^{-1}). The maps with average TrC NO_2 are shown and described in Section 3.3. The same quality assurance threshold (0.75) and re-gridding technique was used as for the complete TROPOMI time series. To account for seasonality and differences in NO_2 between months, we also calculated TROPOMI NO_2 anomalies for 2018-2022. The first step was computing a climatology for every month by averaging all days during

the TROPOMI record for each individual month. Next, we separated the calm wind days by month and for each calculated the percent TrC NO_2 difference between the individual day and the climatology for the same month. Over the roughly 4.5 years of TROPOMI's data record, there were 450 individual calm wind day NO_2 anomalies calculated. An average was taken of this set of anomalies to obtain a single gridded anomaly (see Section 3.3) that describes the enhancement or reduction of NO_2 over each grid cell that also accounts for seasonal changes in NO_2 amounts.

3. Results

3.1 Satellite NO_2 Time Series

Figure 4 shows the 2004-2022 OMI time series for the three boxes defined in Figure 2. The red dashed trend lines were calculated from the 12-month moving averages to remove NO_2 seasonality. In the Houston, TX area (Figure 3a), the time series exhibits large seasonal fluctuations, in most cases over a factor of two from the winter to summer months. This is typically due to the differences in NO_2 lifetime in winter and summer months. The lifetime varies from 2 to 5hr during the daytime in summer (Beirle et al., 2011) and 12–24 hr during winter (Shah et al., 2020). The amplitudes of the peaks are noticeably higher in the first four years (2005-2009) of the time series compared to the most recent decade. There is an overall negative trend of -0.027± 0.0055 DU per decade with 13.7% decrease per decade, much of it due to the reduction of NO_2 in the first 5 years of the time series. Similar trends are also observed in urban areas throughout the U.S (Lamsal et al., 2015; Krotkov et al., 2016, Goldberg et al., 2021). After 2010, the NO_2 remains relatively constant. Over the entire time series the average value is 0.153 DU and this average value is closer to the minima of the NO_2 annual cycles due to the troughs of the annual cycle lasting several months, as opposed to 1-3 month peaks in winter.

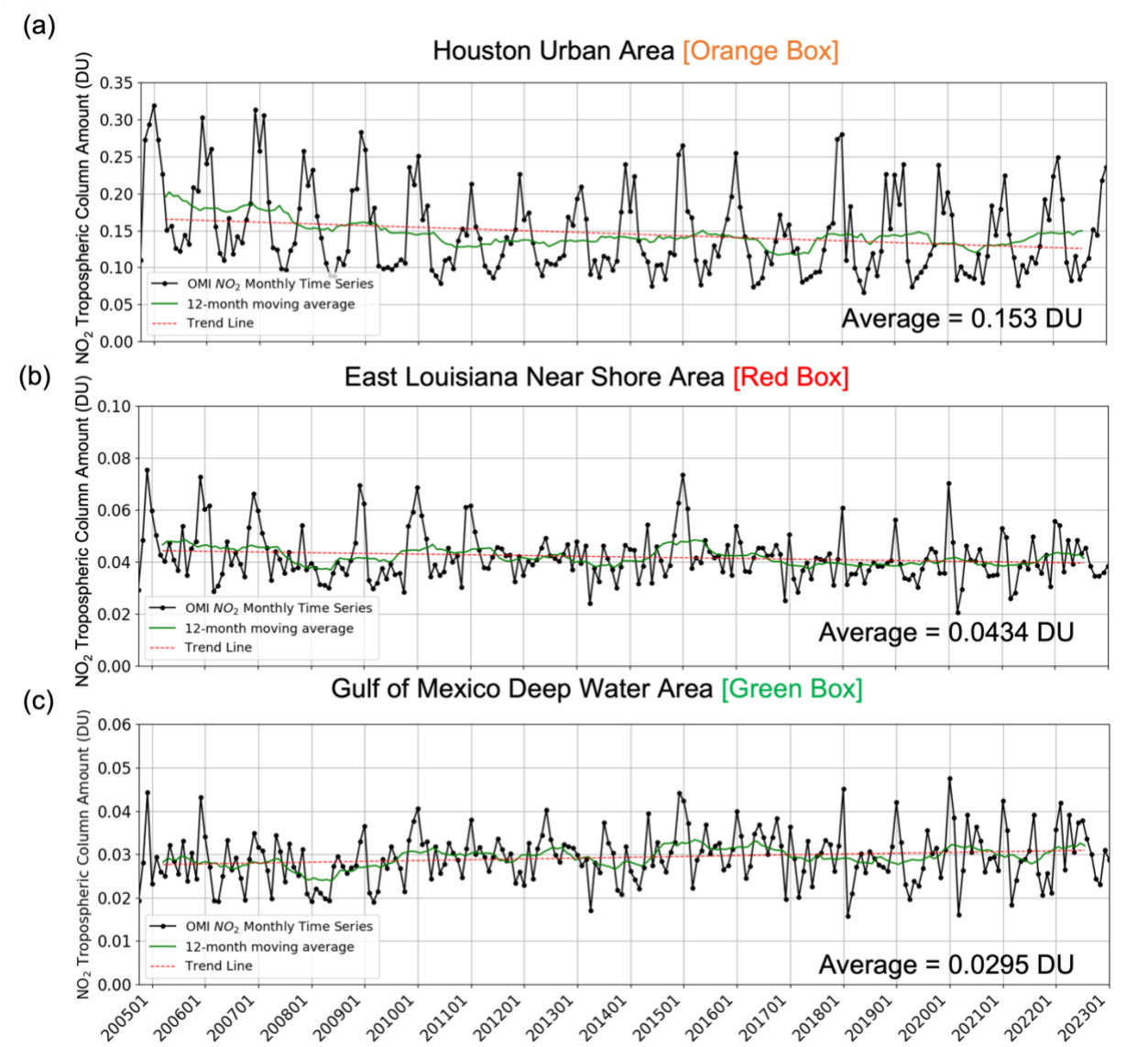

Figure 4: Time series of OMI TrC NO_2 monthly averages for the boxes shown in Figure 2, between late 2004 and 2022: (a) Houston, TX urban area (orange on Figure 2), (b) Near-shore (red on Figure 2), (c) GOM deepwater area in the GOM (green on Figure 2). The 12-month moving average (green line) and the linear trend line (dashed red) over the time series are also plotted.

Unlike the urban area, in the near shore area (Figure 4b) there is a less-defined NO_2 seasonality at the coast and over water. Although peaks and troughs in column NO_2 exist in 2005-2010, thereafter the time series becomes highly variable from month to month. The trend in this region was -0.0022± 0.0008 DU per decade (5.8% decrease per decade), and while still negative, is a lower magnitude than that of Houston by a factor of 10. The negative trend indicates the influence of relatively polluted land areas to the north, such as New Orleans; however, with fewer significant local sources, the potential for trends resulting from NO_2 emissions reductions is lower over-water. The average value for the near shore region is 0.0434 DU, about 28% of the urban Houston area value. It is important to note that while OMI can be

useful for remote sensing over water (e.g., Thompson et al., 2023), the data tend to be noisy on a day to day basis.

The deepwater area is characterized by a noisy time series with no discernable seasonal pattern (Figure 4c). Since all pixels in the box are used to calculate the average column amount value for each month, the influences of deepwater ONG operations in this area, which are relatively small compared to the pixel size, are likely washed out. In Section 3.3 we also show time series for NO_2 hotspots over individual ONG platforms without including the rest of the deepwater area. The overall average value in the deepwater area was 0.0295 DU, around 67% that of the near shore area and 19% of Houston. There is a slight increase of 5.4% per decade in this area with a positive trend (0.00189± 0.00054 DU per decade). The positive trend may result solely from noise due to the low NO_2 column amounts. However, we also note that there was an increase in deepwater ONG operations in the last decade which could have contributed to this trend (Section 3.3). Only the Houston trend is statistically significant given that the 95% confidence interval indicates an error uncertainty of 5.5%. For the near shore and deepwater areas, the uncertainty is around 30% for each. Given the higher uncertainty and smaller trend values, we cannot make a conclusive determination on whether the ONG activity drives these trends.

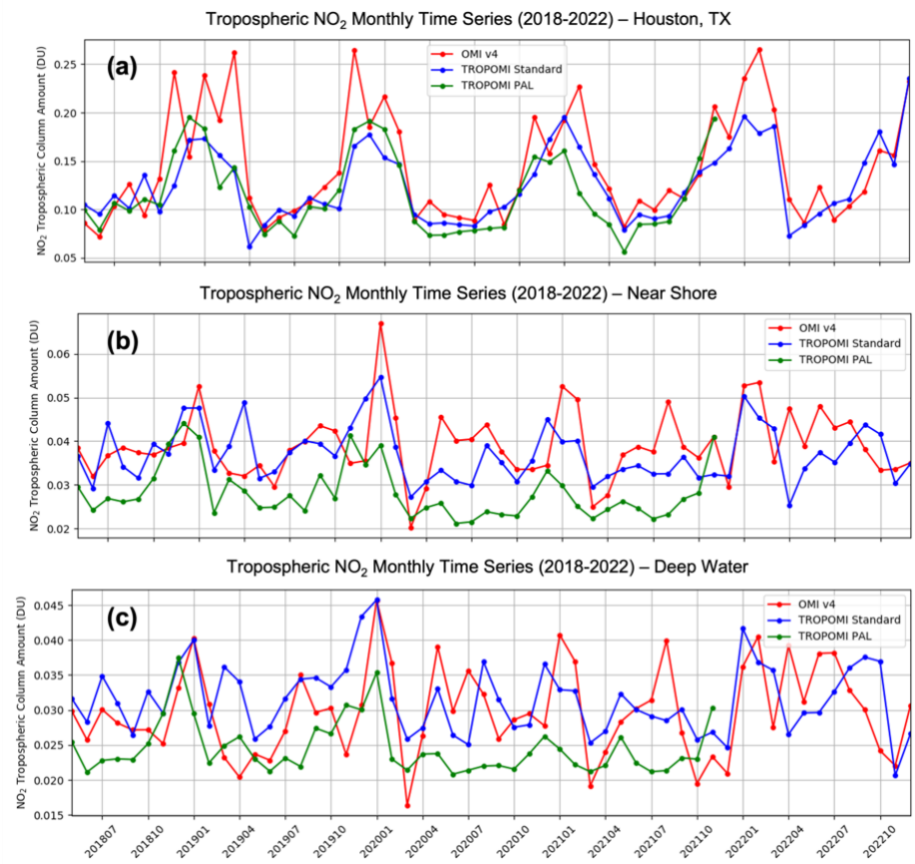

Figure 5: Comparisons of the 2018-2022 TrC NO_2 time series from OMI v4, the standard TROPOMI product and the reprocessed TROPOMI PAL product for a) Houston, TX urban area, (b) Near-shore, (c) GOM deepwater area in the GOM. Note that the TROPOMI PAL dataset is currently only available through 2021.

We calculated the NO_2 time series from all three satellite datasets over our three regions to provide context for the values described above. The time series of OMI, standard TROPOMI, and the TROPOMI PAL datasets (Figure 5) from 2018-2022 show how the observations differ. OMI averages 7.5% and 4.5% higher than TROPOMI in the near shore (Figure 5b) and deepwater areas (Figure 5c), respectively. This makes sense given that in the urban area OMI is clearly higher than TROPOMI observations on average (Figure 5a). These time series also show that the standard TROPOMI product is consistently higher than the PAL by around 21.5% in the deepwater box and 15.7% in the near shore box. The difference between the PAL and standard TROPOMI dataset was not found to be large over a polluted area like Houston, with the standard product being on average within 10% of the PAL between mid-2018 and late 2021.

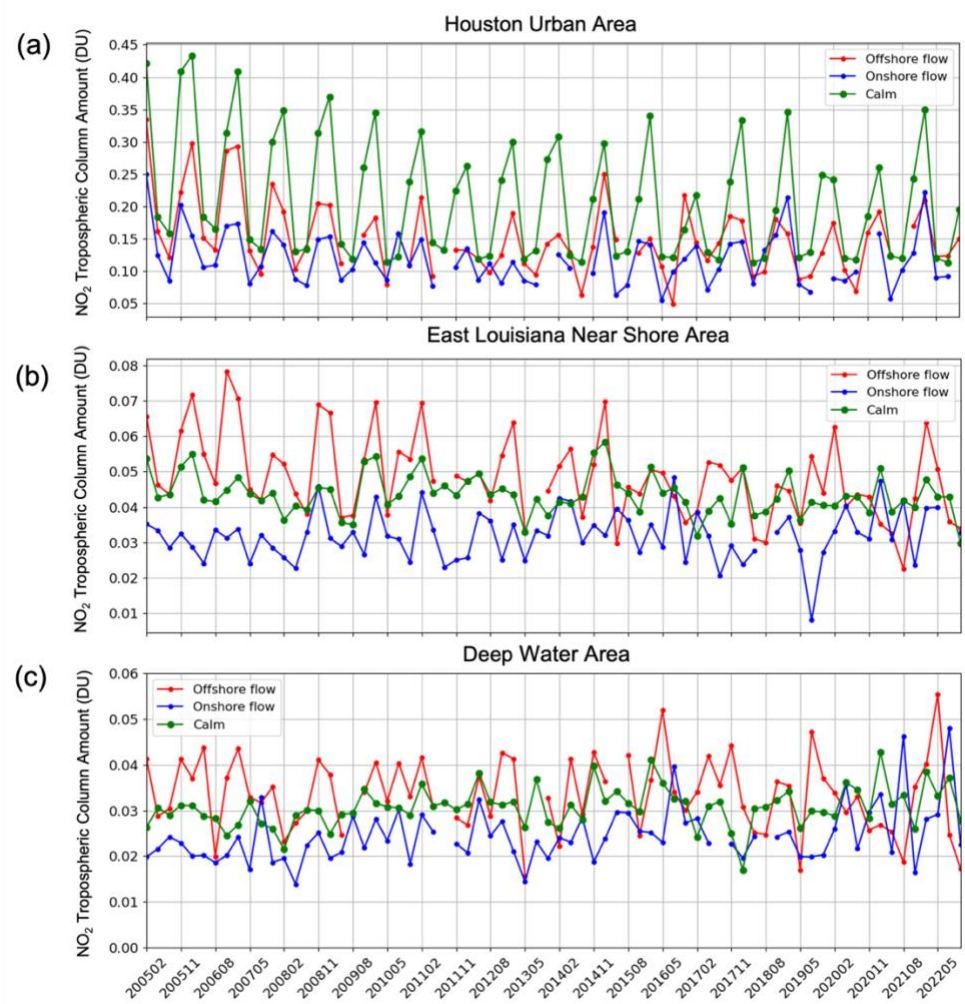

Figure 6: Time series of OMI TrC NO_2 seasonal averages based on wind condition, for: (a) Houston, TX urban area, (b) Near-shore, and (c) GOM deepwater area. The three conditions for (b) and (c) are: MERRA-2 950 hPa winds > 10 ms^{-1} from the south quadrant (blue line), winds > 10 ms^{-1} from the north quadrant (red line) and winds less than 5 ms^{-1} from any direction (green line). For (a), the directions were adjusted to southwest (blue) and northwest (red) quadrants respectively.

3.2 Wind-based Time Series

The time series, with the influence of different wind conditions described in Section 2, are displayed in Figure 6. Missing points are the 3-month time periods when there were not enough days to meet the wind conditions (at least 10). For the Houston area (Figure 6a), calm winds clearly result in the highest average NO_2 column amount (0.207 DU) because there is little transport of emissions away from the city. This is about a 35% increase above the average of the entire Houston time series (Figure 4a). Offshore flow (wind from other land areas toward the GOM) produces an average monthly column amount of 0.151 DU, while onshore flow results in an average value of 0.118 DU. This indicates that for the most part offshore sources do not impact onshore areas given their small magnitude of NO_x emission. As expected, in the near shore and deepwater areas (Figure 6b and 6c), the calm wind time series fall in between the offshore and onshore wind time series. The trends of the calm wind case in near shore and deepwater areas are -0.0027 DU per decade and 0.0021 DU per decade respectively. Although these NO_2 amounts and trends are relatively small, this equates to a total increase of 13.5% for the deepwater area, and 8.5% decrease for the near shore area over the OMI record. The NO_2 trends corresponding to calm wind conditions can also better describe trends over ONG operations since we eliminate days with significant transport of clean or polluted air masses. Average TrC NO_2 amount for the onshore flow case in the deepwater was 0.024 DU which can be considered very close to a typical background value over clean marine areas. For the calm wind case the average value was 0.032 DU, only slightly lower than the offshore case (0.0335 DU). The small difference between the two can be partially explained by the significant dip in 2020 for the offshore flow case, most likely due to the COVID-19 lockdowns. Table 1 summas the average column amounts for the original time series and wind-based time series. For the near shore and deepwater areas, the calm wind time series averages were close to the overall average.

Table 1: Average OMI Column TrC NO_2 for the wind-based time series and the original time series.

Time Series NO_2 Tropospheric Column Amount Averages (DU)

Wind condition	Urban	Near shore	Deepwater
Offshore flow	0.151	0.0495	0.0335
Onshore flow	0.118	0.0307	0.0231
Calm	0.209	0.0440	0.0307
None (all days)	0.153	0.0434	0.0295

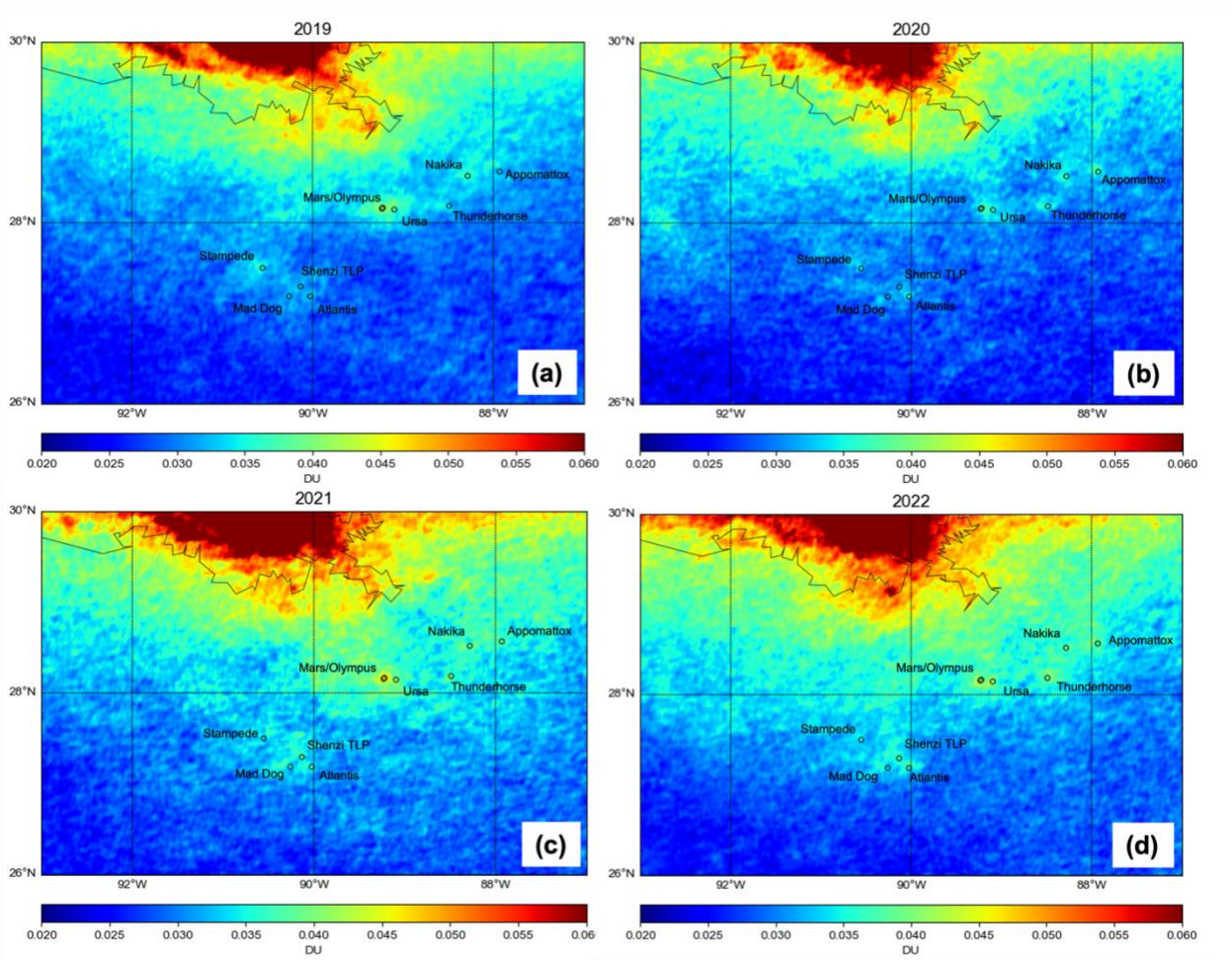

Figure 7: TROPOMI tropospheric NO_2 column averages for (a) 2019, (b) 2020, (c) 2021 and (d) 2022. The averages were calculated using only the days on which MERRA-2 950 hPa winds at 18 UTC were less than 5 ms^{-1}. Pixels with a QA value of less than 0.75 were excluded during the averaging process.

3.3 Hotspots identified by TROPOMI

Aside from analyzing the long-term satellite record of the three areas, we also aimed to assess how well TROPOMI can observe ONG hotspots. The maps in Figure 7a-d show TROPOMI TrC NO_2 averages for each year in 2019-2022. These averages were calculated using only days for the calm wind case (MERRA-2 winds < 5 ms^{-1}) because this yields the best chance at isolating NO_2 hotspots from the surrounding areas. One noticeable difference from year to year is the varying levels of TrC NO_2, both over background and polluted regions. For instance, 2021 had an overall higher background and near shore NO_2 amounts than other years. In 2020, the average offshore amounts were lower, possibly due to restrictions of the COVID-19 pandemic (Bauwens et al., 2021; Fioletov et al., 2022). We identified several hotspots from these maps, shown as an average from mid-2018 through 2022 (Figure 8). The NO_2 hotspots correspond to one or more platforms in the 2017 BOEM emissions inventory.

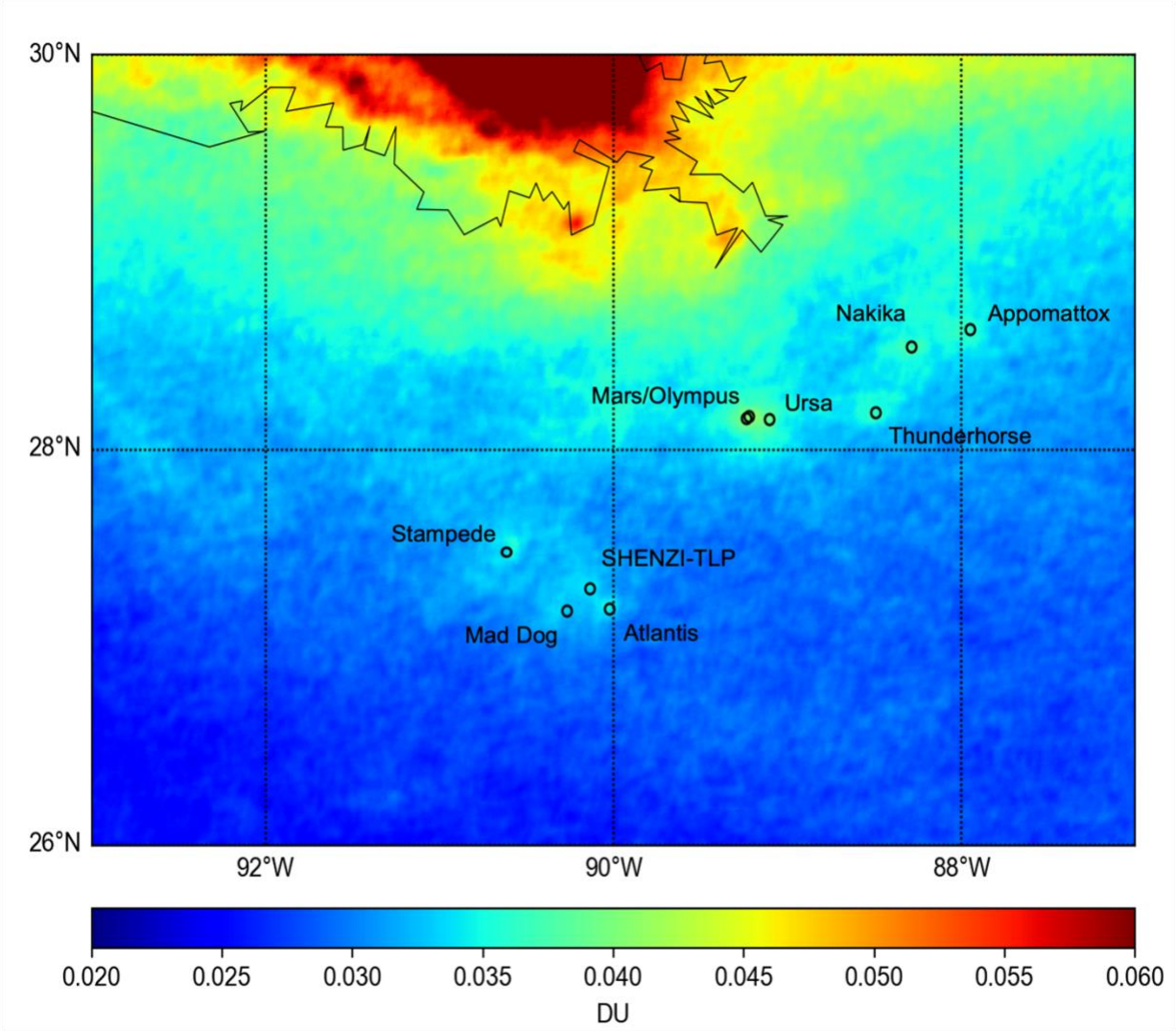

Figure 8: 2018-2022 tropospheric NO_2 column averages from TROPOMI, using only days on which MERRA-2 950 hPa winds at 18 UTC were less than 5 ms^{-1}. The circles and labels show locations of key platforms contributing to the NO_2 column hotspots.

The largest hotspot consists of the Mars and Olympus platforms, both located around 89.22° W and 28.17° N. It is visible clearly in every map in Figure 7. Ursa [89.104° W, 28.154° N], a platform roughly 10 km to the east, also contributes to this hotspot. Other platforms which can be identified are Thunderhorse [88.496° W, 28.19° N], Nakika [88.289° W, 28.521° N], and Appomattox [87.95° W, 28.61° N]. Appomattox only began operations in May 2019, and is visible for every year since 2019. Although located further south in the deepwater region, the Atlantis platform [90.027° W, 27.195° N], in addition to Mad Dog [90.269° W, 27.188° N] and SHENZI-TLP [90.135° W, 27.301° N] platforms all form visible hotspots in the same region on the TROPOMI maps. The hotspot to the northwest of Mad Dog, seen clearly at 90.6° W and 27.5° N is from Stampede, another deepwater platform. It began production in 2018 and so it, like Appomattox, is not included in the BOEM 2017 inventory. The aforementioned platforms are all in the top twenty largest NO_x emitters in the GOM according to the BOEM 2017 inventory, with exception of Stampede and Appomattox, the newer platforms that are not in the inventory. Numerous shallow water platforms are located above 28.5° N closer to the coast;

however, the individual platforms are generally low-NO_x emitters and are more difficult to distinguish from the background NO_2 values in the near-shore area. The Mars/Olympus hotspot represents a 25% increase above background levels of the deepwater area. Other platforms had smaller enhancements: Appomattox, Stampede, Thunderhorse and Atlantis had 13%, 7.7%, 8.1% and 6.9% higher NO_2 than background levels respectively. The hotspot enhancements were calculated by comparing the wind-based time series of each specific hot spot with the deepwater area time series (Figure 9).

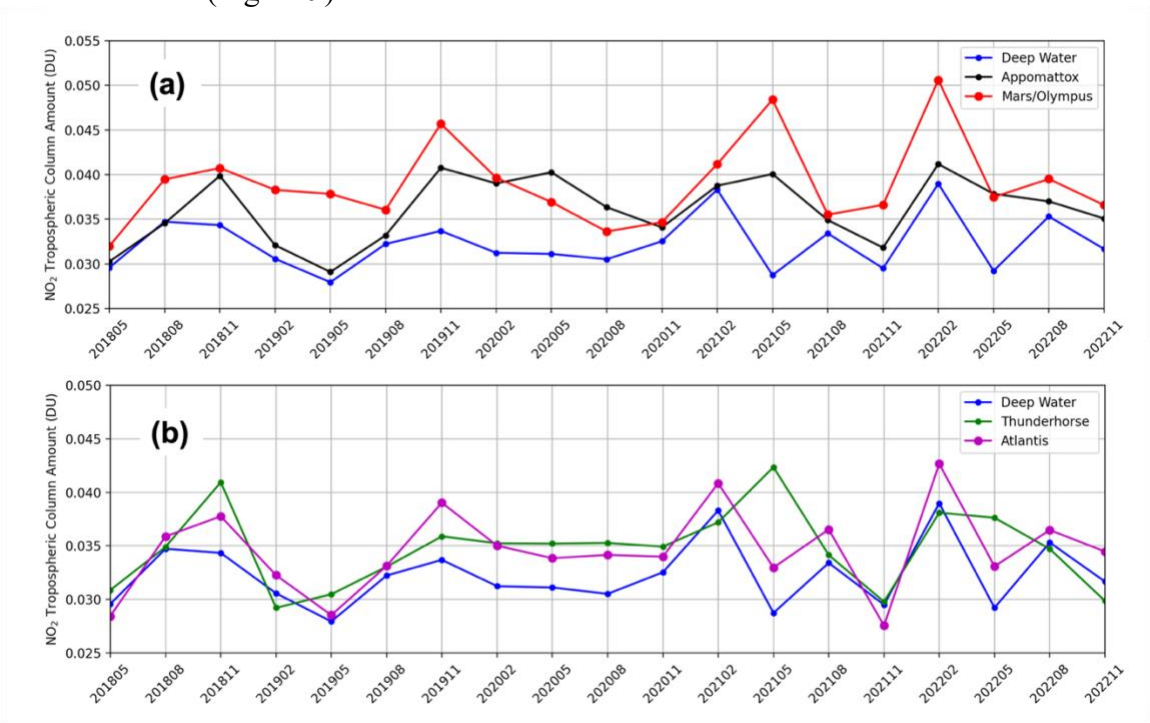

Figure 9: Three-month time series for (a) the Appomattox and Mars/Olympus hotspots compared with the deepwater box (green box in Figure 2), and (b) Atlantis and Thunderhorse hotspots compared with the deepwater box. All of the time series were calculated with the calm wind case evaluated at each respective hotspot.

Time series for the hotspots were calculated with the same method as before, except the TROPOMI pixels used were restricted to within ± 0.1 degrees longitude and latitude of the platform coordinates. Given the distance of deepwater platforms from shore and the NO_2 column amounts being relatively small compared to that of polluted land areas, it is doubtful they produce any significant effects on coastal air quality. For reference, the Mars/Olympus hotspot maximum three-month value is only around 0.05 DU (Figure 9a). Nonetheless, observing these hotspots is important for evaluating the NO_2 budget over the GOM and ultimately validating the NO_x emissions inventories in the future. The NO_2 calm wind anomalies (Figure 10) provide another way to visualize the hotspots. Figure 10 is the average TrC NO_2 percent difference for each 0.01° by 0.01° grid cell between each calm wind day and its respective NO_2 monthly climatology. The same hotspots are visible in the map, the largest of which is Mars/Olympus. The percent anomaly for this hotspot is 9.8%, meaning that calm winds cause the accumulation of an additional 9.8% TrC NO_2 over Mars/Olympus compared to other days. The second and third largest calm wind anomalies are Nakika and Atlantis with 8.5% and 7.8% respectively. A large band of positive NO_2 anomalies stretches across the shallow waters over the area with a

high density of platforms (Figure 10). This is easier to see in the anomaly map rather the overall TROPOMI NO_2 average in Figure 9.

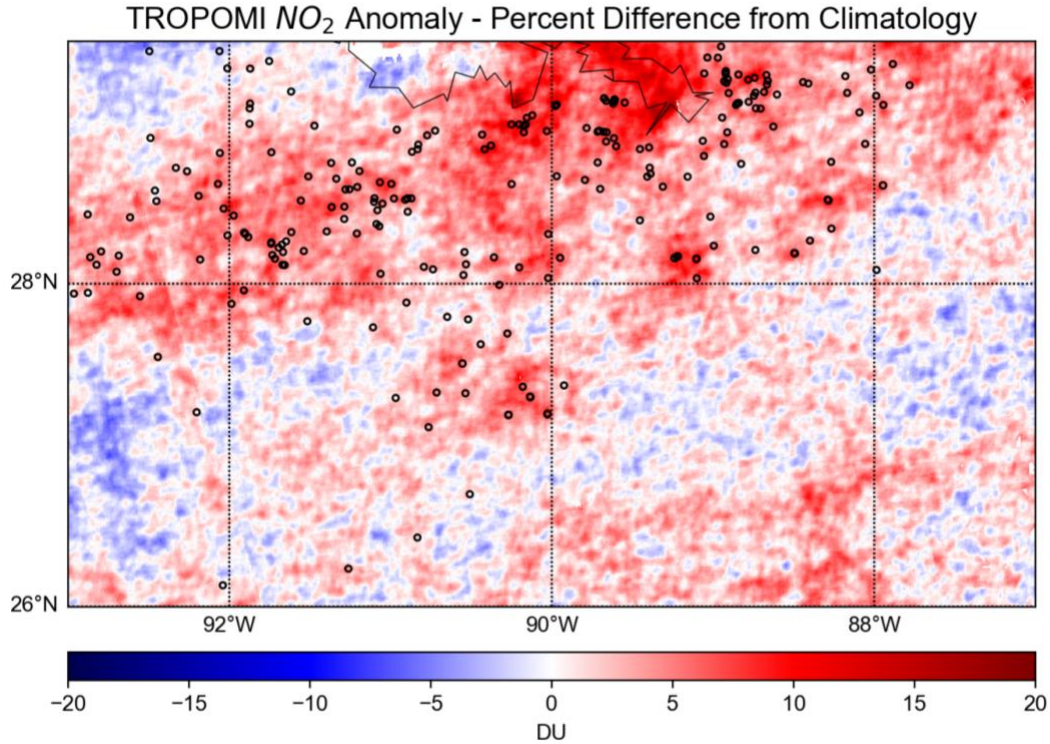

Figure 10: Average TrC NO_2 anomalies from TROPOMI corresponding to calm wind days. The top 250 NO_x emitting platforms from the BOEM 2017 inventory are plotted on the map with empty circles. The TROPOMI data record from May 2018 through December 2022 was used in the calculation and the anomalies were calculated with respect to monthly climatology.

4. Conclusions

We examined the 18+ year record of OMI satellite TrC NO_2 in the GOM region. Three areas were considered for time series analysis: 1) Houston urban, 2) near shore and 3) deep water. A trend analysis on the time series revealed a negative NO_2 trend for the Houston and near shore areas and a slight increasing trend for the deepwater area. The average column amount of the time series for Houston (0.148 DU) was three times greater that of the near shore area (0.0434 DU) which indicates the air over water is clean in comparison, despite the presence of offshore ONG activity. The wind-classified time series showed that ONG activity does have an impact on the NO_2 amount in deepwater region. For instance, in the calm wind case the NO_2 columns were around 33% higher on average than the onshore (wind from the south) case. The calm wind trend for the deepwater area was +0.0021 DU per decade, indicating that there could be a slight increase in NO_x emissions from deepwater ONG platforms since 2005.

We also showed the capability of TROPOMI to observe NO_2 hotspots from oil and natural gas sources in the GOM. On average TROPOMI calm wind case maps, there are clear indications of several NO_2 hotspots in the vicinity of ONG platforms. Visually this is observed mostly in deepwater regions where the background is low enough for the hotspots to be isolated

from the background. The largest hotspot, Mars/Olympus, is 25% above the deepwater background value partly because the two platforms are located only 1.9 km apart. The NO_2 anomalies from monthly climatology during calm wind conditions help quantify relative NO_2 enhancements from ONG operations. Clearly visible are distinct hotspots. Mars/Olympus is the highest, with a 9.8% anomaly for the 2018-2022 TROPOMI record. Positive anomalies are also observed in the shallow water area (north of 28° N) where there are numerous smaller platforms. These platforms, while not clearly identifiable in the TROPOMI NO_2 averages, emit enough NO_x to cause increases above the background values during calm winds.

Given that NO_2 enhancements from emissions can be seen by TROPOMI, a major component of future work will focus on estimating emissions from these hotspots to validate BOEM's ONG NO_x emissions inventories. Liu et al. (2022) and Goldberg et al. 2022) have shown that this can be done without chemical models, using appropriate meteorological data and when a sufficient source signal exists that can be identified in the satellite observations. Presumably their approach can be applied to upcoming data from the TEMPO instrument, which is the first geostationary UV-Vis instrument measuring NO_2 over North America. For validation of TEMPO we will conduct a SCOAPE-II cruise in 2024 with Pandora and in-situ measurements as in Thompson et al. (2023). The work presented here provides the first insight into long-term trends over the GOM and demonstrates the capability of higher-resolution satellite instruments to observe NO_2 hotspots, even over sources with comparatively smaller emissions and spatial footprint than urban areas. Note that TEMPO can monitor ONG emissions as well as mobile marine and land-based NO_x sources hour-by-hour throughout the GOM region. These processes interact throughout the boundary layer NO_2 (Sullivan et al., 2023), contributing to the cycling of reactive nitrogen across a range of environments, e.g., urban business, residential, shipping lanes, ports, the vast petrochemical enterprise and wetlands.

Acknowledgements

This study was partially funded by the U.S. Department of the Interior, Bureau of Ocean Energy Management through Interagency Agreement M23PG00001with NASA (R. Stauffer, PI). Disclaimer: This report has been technically reviewed by BOEM, and it has been approved for publication. The views and conclusions contained in this document are those of the authors and should not be interpreted as representing the opinions or policies of the U.S. Government, nor does mention of trade names or commercial products constitute endorsement or recommendation for use. This research is also supported by an appointment to the NASA Postdoctoral Program at NASA Goddard Space Flight Center, administered by ORAU through a contract with NASA.

Data Availability

OMI total and tropospheric column NO_2 data can be downloaded from NASA GES DISC at https://aura.gesdisc.eosdis.nasa.gov/data/Aura_OMI_Level2/OMNO2.003 (https://doi.org/10.5067/Aura/OMI/ DATA2017; Krotkov et al., 2019). The high resolution OMI dataset is a research data product developed by Lok Lamsal and can be downloaded from: https://avdc.gsfc.nasa.gov/pub/data/satellite/Aura/OMI/V03/L3/OMNO2d_HR/OMNO2d_HRM/ TROPOMI tropospheric NO_2 column data is obtained from the Copernicus Hub at https://scihub.copernicus.eu/ (https:// doi.org/10.5270/S5P-s4ljg54; Copernicus Sentinel-5P, 2019 & 2021). The MERRA-2 data are available from GES DISC at https://disc.gsfc.nasa.gov/datasets/M2I3NPASM_5.12.4/summary (doi:10.5067/QBZ6MG944HW0; GMAO, 2015). All analyses and creation of figures were performed using publicly available Python modules.

References

Bauwens, M., Compernolle, S., Stavrakou, T., Müller, J. F., van Gent, J., Eskes, H., et al. (2020): Impact of coronavirus outbreak on NO_2 pollution assessed using TROPOMI and OMI observations, Geophys. Res. Lett., 47, https://doi.org/10.1029/2020GL087978.

Beirle, S., Platt, U., Wenig, M., & Wagner, T. (2003). Weekly cycle of NO2 by GOME measurements: A signature of anthropogenic sources. *Atmospheric Chemistry and Physics*, 3(6), 2225– 2232. https://doi.org/10.5194/acp-3-2225-2003.

Boersma, K. F., Eskes, H. J., & Brinksma, E. J. (2004). Error analysis for tropospheric NO_2 retrieval from space. *Journal of Geophysical Research,* 109(D4), https://doi.org/10.1029/2003JD003962.

Boersma, K. F., Eskes, H. J., Veefkind, J. P., Brinksma, E. J., van der A, R. J., Sneep, M., Bucsela, E. J. (2007). Near-real time retrieval of tropospheric NO_2 from OMI. *Atmospheric Chemistry and Physics*, 7, 2103– 2118. https://doi.org/10.5194/acp-7-2103-2007.

Burrows, J. P., Weber, M., Buchwitz, M., Rozanov, V., Ladstatter-Weibenmayer, A., Richter, A., et al. (1999). The global ozone monitoring experiment (GOME): Mission concept and first scientific results. *Journal of Atmospheric Sciences*, **56**, 151– 175.

Bell, M. L., Peng, R. D., & Dominici, F. (2006). The exposure-response curve for ozone and risk of mortality and the adequacy of current ozone regulations. *Environmental Health Perspectives*, 114(4), 532– 536. https://doi.org/10.1289/ehp.8816.

Choi, S., Lamsal, L. N., Follette-Cook, M., Joiner, J., Krotkov, N. A., Swartz, W. H., et al. (2020): Assessment of NO_2 observations during DISCOVER-AQ and KORUS-AQ field campaigns, Atmos. Meas. Tech., 13, 2523–2546, https://doi.org/10.5194/amt-13-2523-2020.

Copernicus Sentinel data processed by ESA, Koninklijk Nederlands Meteorologisch Instituut (KNMI) (2019), Sentinel-5P TROPOMI Tropospheric NO2 1-Orbit L2 5.5km x 3.5km, Greenbelt, MD, USA, Goddard Earth Sciences Data and Information Services Center (GES DISC), Accessed: March 2023, https://doi.org/10.5270/S5P-s4ljg54.

Copernicus Sentinel data processed by ESA, Koninklijk Nederlands Meteorologisch Instituut (KNMI) (2021), Sentinel-5P TROPOMI Tropospheric NO2 1-Orbit L2 5.5km x 3.5km, Greenbelt, MD, USA, Goddard Earth Sciences Data and Information Services Center (GES DISC), Accessed: March 2023, https://doi.org/10.5270/S5P-9bnp8q8.

Duncan, B. N. (2020) NASA resources to monitor offshore and coastal air quality. Sterling (VA): U.S. Department of the Interior, Bureau of Ocean Energy Management. OCS Study BOEM 2020-046. 41 p.

Dacic, N., Sullivan, J. T., Knowland, K. E., et al. (2020). Evaluation of NASA's high-resolution global composition simulations: Understanding a pollution event in the Chesapeake Bay during the summer 2017 OWLETS campaign. *Atmospheric Environment*, 222, https://doi.org/10.1016/j.atmosenv.2019.117133.

Fioletov, V., McLinden, C. A., Griffin, D., Krotkov, N., Liu, F., and Eskes, H (2022).: Quantifying urban, industrial, and background changes in NO_2 during the COVID-19 lockdown period based on TROPOMI satellite observations, Atmos. Chem. Phys., 22, 4201–4236, https://doi.org/10.5194/acp-22-4201-2022.

Gelaro, R., McCarty, W., Suárez, M. J., et al. (2017). The Modern-Era Retrospective Analysis for Research and Applications, version 2 (MERRA-2). *Journal of Climate*, **30**(14), 5419– 5454. https://doi.org/10.1175/JCLI-D-16-0758.1

Global Modeling and Assimilation Office (GMAO) (2015), MERRA-2 inst3_3d_asm_Np: 3d,3-Hourly,Instantaneous,Pressure-Level,Assimilation,Assimilated Meteorological Fields V5.12.4, Greenbelt, MD, USA, Goddard Earth Sciences Data and Information Services Center (GES DISC), Accessed: Jan 2023, https://doi.org/10.5067/QBZ6MG944HW0.

Goldberg, D.L.; Anenberg, S.C.; Kerr, G.H.; Mohegh, A.; Lu, Z.; Streets, D.G. (2021): TROPOMI NO_2 in the United States: A detailed look at the annual averages, weekly cycles, effects of temperature, and correlation with surface NO_2 concentrations. *Earth's Futur*, *9*, https://doi.org/10.1029/2020EF001665.

Goldberg, D. L., Harkey, M., de Foy, B., Judd, L., Johnson, J., Yarwood, G., and Holloway, T. (2022): Evaluating NO_x emissions and their effect on O_3 production in Texas using TROPOMI NO_2 and HCHO, Atmos. Chem. Phys., 22, 10875–10900, https://doi.org/10.5194/acp-22-10875-2022.

Herman, J., Cede, A., Spinei, E., et al. (2009): NO_2 column amounts from ground-based Pandora and MFDOAS spectrometers using the direct-sun DOAS technique: Intercomparisons and application to OMI validation, J. Geophys. Res., 114, D13307, https://doi.org/10.1029/2009JD011848.

Jensen, M. P., Flynn, J. H., Judd, L. M., Kollias, P., Kuang, C., Mcfarquhar, G., et al. (2022). A succession of cloud, precipitation, aerosol, and air quality field experiments in the coastal urban environment. Bulletin of the American Meteorological Society, 103(2), 103– 105. https://doi.org/10.1175/bams-d-21-0104.1.

Judd, L. M., Al-Saadi, J. A., Janz, S. J, et al. (2019): Evaluating the impact of spatial resolution on tropospheric NO_2 column comparisons within urban areas using high-resolution airborne data, Atmos. Meas. Tech., 12, 6091–6111, https://doi.org/10.5194/amt-12-6091-2019.

Judd, L. M., Sullivan, J. T., Lefer, B., Haynes, J., Jensen, M. P., & Nadkarni, R. (2021). TRACER-AQ science plan: An interagency cooperative air quality field study in the Houston, TX Metropolitan Region. Retrieved from https://www-air.larc.nasa.gov/missions/tracer-aq/docs/TRACERAQ_SciencePlan_v1.pdf

Kollonige, D. E., Thompson, A. M., Josipovic, M., et al. (2018). OMI satellite and ground-based Pandora observations and their application to surface NO_2 estimations at terrestrial and marine sites. J. Geophys. Res., 123, 1441-1459, https://doi.org/10.1002/2017JD026518.

Kotsakis, A., Sullivan, J. T., Hanisco, T. F., Swap, R. J., Caicedo, V., Berkoff, T. A., et al. (2022). Sensitivity of total column NO_2 at a marine site within the Chesapeake Bay during OWLETS-2. *Atmospheric Environment*, 277, 119063. https://doi.org/10.1016/j.atmosenv.2022.119063

Levelt, P., Van den Oord, G., Dobber, M., et al. (2006). The ozone monitoring instrument, IEEE Transactions on Geosci, and Remote Sensing*, 44*(5), 1093-1101.

Levelt, P. F., Joiner, J., Tamminen, J., et al. (2018) The ozone monitoring instrument: Overview of 14 years in space, Atmospheric Chemistry and Physics, 18(8):5699–5745, https://doi.org/10.5194/acp-18-5699-2018.

Lamsal, L. N., Duncan, B. N., Yoshida, Y., Krotkov, N. A., Pickering, K. E., Streets, D. G., & Lu, Z. (2015). U.S. NO_2 trends (2005–2013): EPA air quality system (AQS) data versus improved observations from the ozone monitoring instrument (OMI). *Atmospheric Environment*, 110, 130– 143. https://doi.org/10.1016/j.atmosenv.2015.03.055.

Lamsal, L. N., Krotkov, N. A., Vasilkov, A., et al. (2021): Ozone Monitoring Instrument (OMI) Aura nitrogen dioxide standard product version 4.0 with improved surface and cloud treatments, Atmos. Meas. Tech., 14, 455–479, https://doi.org/10.5194/amt-14-455-2021.

Liu, F., Tao, Z., Beirle, et al. (2022): A new method for inferring city emissions and lifetimes of nitrogen oxides from high-resolution nitrogen dioxide observations: a model study, Atmos. Chem. Phys., 22, 1333–1349, https://doi.org/10.5194/acp-22-1333-2022.

Krotkov, N. A., McLinden, C. A., Li, C., Lamsal, L. N., Celarier, E. A., Marchenko, S. V., Swartz, W. H, et al. (2016): Aura OMI observations of regional SO_2 and NO_2 pollution changes from 2005 to 2015, Atmos. Chem. Phys., 16, 4605–4629, https://doi.org/10.5194/acp-16-4605-2016.

Krotkov, N. A., Lamsal, L. N., Marchenko, S. V., Bucsela, E. J., Swartz, W. H., & Joiner, J., & The OMI Core Team. (2019). OMI/Aura nitrogen dioxide (NO2) total and tropospheric column 1-orbit L2 swath 13x24 km V003. Goddard Earth Sciences Data and Information Services Center (GES DISC). Accessed Sept. 2022. https://doi.org/10.5067/Aura/OMI/DATA2017

Martins, D. K., Najjar, R. G., Tzortziou, M., Abuhassan, N., Thompson, A. M., & Kollonige, D. E. (2016). Spatial and temporal variability of ground and satellite column measurements of NO_2 and O_3 over the Atlantic Ocean during the deposition of atmospheric nitrogen to coastal ecosystems experiment (DANCE). *Journal of Geophysical Research*, 121(23), 14,175– 14,187. https://doi.org/10.1002/2016JD024998

Munro, R., Lang, R., Klaes, D., Poli, G., Retscher, C., Lindstrot, R., et al. (2016): The GOME-2 instrument on the Metop series of satellites: instrument design, calibration, and level 1 data processing – an overview, Atmos. Meas. Tech., 9, 1279–1301, https://doi.org/10.5194/amt-9-1279-2016.

Nowlan, C. R., Liu, X., Leitch, J. W. (2016): Nitrogen dioxide observations from the Geostationary Trace gas and Aerosol Sensor Optimization (GeoTASO) airborne instrument: Retrieval algorithm and measurements during DISCOVER-AQ Texas 2013, *Atmospheric Measurement Techniques,* 9, 2647–2668, https://doi.org/10.5194/amt-9-2647-2016.

Nowlan, C. R., Liu, X., Janz, S. J., Kowalewski, M. G., Chance, K., Follette-Cook, M. B., et al. (2018): Nitrogen dioxide and formaldehyde measurements from the GEOstationary Coastal and Air Pollution Events (GEO-CAPE) Airborne Simulator over Houston, Texas, Atmos. Meas. Tech., 11, 5941–5964, https://doi.org/10.5194/amt-11-5941-2018.

Piters, A. J. M., Boersma, K. F., Kroon, M., Hains, J. C., Van Roozendael, M., Wittrock, F., Abuhassan, N, et al. (2012): The Cabauw Intercomparison campaign for Nitrogen Dioxide measuring Instruments (CINDI): design, execution, and early results, Atmos. Meas. Tech., 5, 457–485, https://doi.org/10.5194/amt-5-457-2012.

Reed, A. J., Thompson, A. M., Kollonige, D. E., Martins, D. K., Tzortziou, M. A., Herman, J. R., et al. (2015): Effects of local meteorology and aerosols on ozone and nitrogen dioxide retrievals from OMI and pandora spectrometers in Maryland, USA during DISCOVER-AQ 2011, *J. Atmos. Chem*., 72, 455–482, https://doi.org/10.1007/s10874-013-9254-9.

Richter, A., & Burrows, J. P. (2002). Tropospheric NO2 from GOME measurements. *Advances in Space Research*, 29, 1673– 1683, https://doi.org/10.1016/S0273-1177(02)00100-X.

Richter, A., Begoin, M., Hilboll, A., and Burrows, J. P. (2011): An improved NO_2 retrieval for the GOME-2 satellite instrument, Atmos. Meas. Tech., 4, 1147–1159, https://doi.org/10.5194/amt-4-1147-2011.

Shah, V., Jacob, D. J., Li, K., Silvern, R. F., Zhai, S., Liu, M., et al. (2020). Effect of changing NOx lifetime on the seasonality and long-term trends of satellite-observed tropospheric NO_2 columns over China. *Atmospheric Chemistry and Physics Discussions*, 20(3), 1483–1495. https://doi.org/10.5194/acp-2019-670.

Sullivan, J. T., Berkoff, T., Gronoff, G., et al. (2018): The ozone water-land environmental transition study (OWLETS): An innovative strategy for understanding Chesapeake Bay pollution events. Bulletin of the American Meteorological Society. https://doi.org/10.1175/BAMS-D-18-0025.

Sullivan, J., Dreessen, T., Berkoff, T., et al. (2020) An overview of NASA's Ozone Water–Land Environmental Transition Study (OWLETS) of the Chesapeake Bay airshed. EM Magazine (Air and Waste Management Assn), October 2020.

Sullivan, J. T., Stauffer, R. M., Thompson, A. M., Tzortziou, M. A., Loughner, C. P., Jordan, C. E., & Santanello, J. A. (2023). Surf, turf, and above the Earth: Unmet needs for coastal air quality science in the planetary boundary layer (PBL). *Earth's Future*, 11, e2023EF003535. https://doi.org/10.1029/2023EF003535

Thompson, A. M., Stauffer, R. M., Boyle, T. P, et al. (2019): Comparison of near-surface NO2 pollution with Pandora total column NO_2 during the Korea-United States Ocean Color (KORUS OC) campaign, 2019, Journal of Geophysical Research: Atmospheres, 124, https://doi.org/10.1029/2019JD030765.

Thompson, A .M., Kollonige, D. E., Stauffer, R.M., et al. (2020): Satellite and shipboard views of air quality along the Louisiana coast: The 2019 SCOAPE (Satellite Coastal and Oceanic Atmospheric Pollution Experiment) cruise, EM Magazine (Air and Waste Management Assn), Oct 2020.

Thompson, A.M., Kollonige, D.E., Stauffer, R.M., et al. (2023): Two air quality regimes in total column NO_2 over the Gulf of Mexico in May 2019: Shipboard and satellite views, Earth and Space Science, https://doi.org/10.1029/2022EA002473Torres, O., Bhartia, P. K., Jethva, H., and Ahn, C. (2018): Impact of the ozone monitoring instrument row anomaly on the long-term record of aerosol products, Atmos. Meas. Tech., 11, 2701–2715, https://doi.org/10.5194/amt-11-2701-2018.

Torres, O., Bhartia, P. K., Jethva, H., and Ahn, C. (2018): Impact of the ozone monitoring instrument row anomaly on the long-term record of aerosol products, Atmos. Meas. Tech., 11, 2701–2715, https://doi.org/10.5194/amt-11-2701-2018.

Tzortziou, M., Herman, J., Cede, A., Loughner, C., Abuhassan, N., Naik, S. (2013): Spatial and temporal variability of ozone and nitrogen dioxide over a major urban estuarine ecosystem. *J. Atmos. Chem.*, 72. https://doi.org/10.1007/s10874-013-9255-8.

Tzortziou, M., Parker, O., Lamb, B., et al. (2018): Atmospheric trace gas (NO_2 and O_3) variability in Korean coastal waters, implications for remote sensing of coastal ocean color dynamics, *Remote Sens.*, 2018, *10,* 1587; https://doi.org/10.3390/rs10101587.

Veefkind, J., Aben, I., McMullan, K., et al. (2012). TROPOMI on the ESA Sentinel-5 Precursor: A GMES mission for global observations of the atmospheric composition for climate, air quality and ozone layer applications. Remote Sens. of Environ., 120, 70–83, https://doi.org/10.1016/j.rse.2011.09.027.

van Geffen, J. H., Eskes, H. J., Boersma, K. F., et al. (2018). TROPOMI ATBD of the total and tropospheric NO_2 data products (issue 1.2.0). Royal Netherlands Meteorological Institute (KNMI), De Bilt, the Netherlands, s5P-KNMI-L2-0005-RP.

van Geffen, J. H., Boersma, K. F., Eskes, H., Sneep, M., ter Linden, M., Zara, M., & Veefkind, J. P. (2020). S5P TROPOMI NO slant column retrieval: method, stability, uncertainties and comparisons with OMI. *Atmospheric Measurement Techniques*, **13**(3), 1315– 1335. https://doi.org/10.5194/amt-13-1315-2020.

Wilson, D., Enoch, S., Mendenhall, S., et al. (2018): User's guide for the 2017 Gulfwide Offshore Activities Data System (GOADS-2017). New Orleans (LA): U.S. Dept. of the

Interior, Bureau of Ocean Energy Management, Gulf of Mexico OCS Region. OCS Study BOEM 2018-038.